Research Square

Preprints are preliminary reports that have not undergone peer review.
They should not be considered conclusive, used to inform clinical practice,
or referenced by the media as validated information.

Formation of insoluble Anderson-type heteropoly molybdates in citrate Ni–Mo and Co–Mo impregnation solutions used to prepare HDS catalysts: Causes and effects on catalytic activity

Sergey V. Budukva

zsm@catalysis.ru

Boreskov Institute of Catalysis SB RAS

Mikhail V. Parfenov

Boreskov Institute of Catalysis SB RAS

Mikhail E. Revyakin

Boreskov Institute of Catalysis SB RAS

Evgenii A. Suprun

Boreskov Institute of Catalysis SB RAS

Elizaveta S. Bykova

Boreskov Institute of Catalysis SB RAS

Daria D. Uvarkina

Boreskov Institute of Catalysis SB RAS

Maxim O. Kazakov

Boreskov Institute of Catalysis SB RAS

Research Article

Keywords: citric acid, heteropolycompounds, precipitate, hydrodesulfurization

Posted Date: August 3rd, 2026

DOI: https://doi.org/10.21203/rs.3.rs-10505740/v1

License: This work is licensed under a Creative Commons Attribution 4.0 International License.
Read Full License

Additional Declarations: No competing interests reported.

Formation of insoluble Anderson-type heteropoly molybdates in citrate Ni–Mo and Co–Mo impregnation solutions used to prepare HDS catalysts: Causes and effects on catalytic activity

Sergey V. Budukva*, Mikhail V. Parfenov, Mikhail E. Revyakin, Evgenii A. Suprun, Elizaveta S. Bykova, Daria D. Uvarkina, Maxim O. Kazakov

Boreskov Institute of Catalysis SB RAS, Novosibirsk 630090, Russia

zsm@catalysis.ru

Abstract

This work investigates the composition of precipitates formed in Co-Mo and Ni-Mo citrate-containing impregnation solutions used for the preparation of hydrotreating catalysts, as well as their effect on catalytic activity. The samples were characterized using a variety of techniques, including XRD, IR spectroscopy, SEM, EDS, and XPS. It was found that the dominant compounds in the precipitates are Anderson-type heteropoly compounds. The results show that Ni–Mo citrate solutions predominantly form Anderson-type ammonium 6-molybdonickelate, whereas Co-Mo citrate solutions form sparingly soluble polymolybdates in the absence of alumina and Anderson-type (ammonium 6-molybdocobaltate and ammonium 6-molybdoaluminate) heteropoly compounds upon contact with γ-Al_2O_3. Catalytic activity was evaluated in the hydrotreating of SRGO. Hydrotreating tests showed that the precipitated heteropoly compounds are transformed during sulfidation into sulfide species and may contribute to the overall HDS performance. Therefore, the higher activity observed for catalysts prepared with precipitate formation is mainly attributed to increased actual metal loading.

Keywords: citric acid, heteropolycompounds, precipitate, hydrodesulfurization

1. Introduction

At the beginning of the 20th century, the method for supporting active metals from impregnation solutions containing organic chelating agents such as EDTA, NTA [1], citric acid (CA) and glycols

[2–4] became widely used for the preparation of commercial hydrotreating catalysts. This method made it possible to obtain catalysts with higher activity than those prepared without chelating agents. Studies have shown that the use of chelating agents significantly reduces the interaction of active metals with the support, which promotes the formation of catalysts containing predominantly the Co-Mo-S phase of type II [5,6]. Chelating agents also allow the preparation of impregnation solutions containing Co(Ni) and/or Mo over a wide pH range and help to avoid the formation of sparingly soluble compounds upon interaction with the support surface. It was also found that catalysts prepared using hydroxycarboxylic acids (citric, malic, gluconic) are more active than those prepared using aminocarboxylic acids (NTA, EDTA) [7]. Among all the major hydroxycarboxylic acids, citric acid (CA) has become the most popular chelating agent for the preparation of impregnation solutions [2,8–10].

Previously, our research group proposed a method for preparing impregnation solutions based on a citrate complex compound with the general formula $[M(H_2O)_x]_2[Mo_4O_{11}(HCitr)_2]$, where M = Co or Ni [11–14]. The method involves the sequential dissolution of citric acid, ammonium heptamolybdate (AHM), and cobalt or nickel salts in water. The CA/Co molar ratio for these systems is 1.3–1.4. Nitrates or acetates of these metals were used as cobalt or nickel salts. This preparation method yields stable solutions that can be stored for several months without precipitate formation. However, in this case, the solution contains a high concentration of NO_3^- or CH_3COO^- anions (1.5-1.65 mol/L). While the presence of these anions does not directly affect the formation of the Co(Ni)MoS phase, it increases the viscosity of the impregnation solutions and causes equipment corrosion during industrial catalyst production. These drawbacks can be avoided by using Co and Ni precursors such as hydroxides ($Co(OH)_2$, $Ni(OH)_2$) or basic cobalt ($CoCO_3 \bullet mCo(OH)_2 \bullet nH_2O$) and nickel ($NiCO_3 \bullet mNi(OH)_2 \bullet nH_2O$) carbonates [15]. Dissolving Co(Ni) hydroxides or basic carbonates in citric acid solutions yields only the corresponding citrates. When using these Co(Ni) precursors to optimize the impregnation solutions preparation technology for commercial use, we observed the fact that, during impregnation of the γ-Al_2O_3 support, precipitates of a light color form in some cases.

Particularly abundant precipitate formation was observed for Ni-Mo solutions, often occurring directly in the solution itself within a few minutes (Fig. S1, S2). Moreover, these precipitates did not dissolve upon the further addition of citric acid.

In industrial hydrotreating catalyst production, vessels with volumes of 5-10 m^3 are used for the preparation and storage of impregnation solutions. Precipitate formation in vessels of such volume poses risks of clogging filters and piping as well as damaging pumps which will inevitably lead to an unscheduled shutdown of the catalysts preparation process. From an economic standpoint, such incidents entail significant costs, including the loss of active metals in the form of insoluble precipitate. Consequently, quality control of solutions and adherence to conditions that prevent precipitate formation are critically important factors in the production process.

In the scientific literature, only isolated mentions of precipitate formation in non-citrate Co-Mo or Ni-Mo solutions have been found. In work [16], the formation of precipitates in impregnation Co-Mo solutions obtained by dissolving cobalt nitrate and ammonium heptamolybdate was observed after two months. The authors identified the compounds in the precipitate by X-ray diffraction as a mixture of $(NH_4)_4(Mo_8O_{24.8})(O_2)\cdot 1.2(H_2O)_2\cdot(H_2O)_4$ (JCPDS card № 88-1326) and $(NH_4)_2Mo_4O_{13}$ (JCPDS card № 80-0756). In another work [17], precipitate formation was observed from Mo, Ni, and Co based solutions prepared without the addition of chelating agents. The authors noted rapid precipitate formation in the Ni-Mo solution (the formation time is not specified), whereas Co-Mo solutions were stable for several hours. Using Raman spectroscopy, the authors determined that the precipitate formed from the Ni-Mo solutions is a sparingly water-soluble Anderson-type heteropoly compound (HPC), $(NH_4)_4NiMo_6H_6O_{24}$. For cobalt solutions, no formation of HPC was detected, and the resulting precipitate was attributed to a mixture of AHM and/or $(NH_4)_4Mo_8O_{26}$ mixture. Similar data were obtained by van Veen et al. [18]. Upon impregnating Al_2O_3 with a concentrated AHM solution, a precipitate formed, which was identified by Raman spectroscopy as ammonium polyoctamolybdate $[(NH_4)_6Mo_8O_{27}]_n$. Later, Payen et al. [19] reinvestigated the deposition of AHM onto Al_2O_3 and found that the precipitate formed during the preparation of

Mo/Al_2O_3 catalysts is ammonium 6-molybdoaluminate $(NH_4)_3[AlMo_6O_{24}H_6]$. Finally, Bergwerff et al. showed that impregnating Al_2O_3 pellets with AHM solutions containing citric acid prevents the formation of $(NH_4)_3[AlMo_6O_{24}H_6]$ [20, 21]. At the same time, information on precipitate formation from citrate impregnation solutions containing Mo and a second metal, Co or Ni, is absent from the scientific literature. Thus, the aim of this work is to determine the composition of precipitates formed in citrate impregnation solutions of CoMo and NiMo, to establish the conditions that allow avoiding precipitate formation, and to investigate the effect of the precipitates on the catalytic activity of sulfide CoMo and NiMo catalysts in the hydrotreating of straight-run gas oil (SRGO).

2. Experimental

2.1 Preparation of impregnation solutions and catalysts

For the synthesis of the catalysts and impregnation solutions, commercial reagents were used without preliminary purification: ammonium heptamolybdate ($(NH_4)_6Mo_7O_{24}*4H_2O$, purity ≥ 99.5%), cobalt hydroxide ($Co(OH)_2$, purity ≥ 99.5%), citric acid ($C_6H_8O_7*H_2O$, CA) and nickel hydroxide ($Ni(OH)_2$, purity ≥ 99.5%). The impregnation solutions were prepared by sequential dissolution of citric acid, cobalt (or nickel) hydroxide, and ammonium heptamolybdate in distilled water preheated to 80 °C. Ammonium heptamolybdate was in all cases added after complete dissolution of the Co or Ni hydroxide in the citric acid solution. We hypothesized that the cause of precipitate formation is related to the concentration of citric acid, which acts as a complexing agent and determines the stability of the solutions. To test this hypothesis, Co-Mo and Ni-Mo solutions with different citric acid contents were prepared. It was found that precipitate formation indeed depends on the amount of citric acid added to the impregnation solution. Precipitate formation can be avoided at CA/Co molar ratios ≥1.5 for Co-Mo solutions and CA/Ni molar ratios ≥1.8 for Ni-Mo solutions, calculated on the basis of citric acid monohydrate $C_6H_8O_7*H_2O$. Eventually, four impregnation solutions with different citric acid concentrations were prepared for further investigation (Table 1). The molybdenum concentration for all solutions was 1.59 mol/L, and the atomic ratios of the metals were Co/Mo = 0.4 and Ni/Mo = 0.33. To obtain guaranteed stable solutions, the citric acid/promoter metal ratios were CA/Co = 1.55

and CA/Ni = 1.8, respectively. Impregnation solutions prone to precipitate formation were prepared similarly, except that the CA/Co(Ni) ratios were lower than those for the stable solutions (Table 1).

Table 1. Parameters of the impregnation solutions and designation of the catalysts prepared on their basis

Impregnation solution	Mo, mol/L	Co, mol/L	Ni, mol/L	CA, mol/L	Ratio CA/Co(Ni)	pH at 25°C	Catalyst designation
Solution-1	1.59	0.633	-	0.753	1.18	5.06	CoMo-1
Solution-2			-	0.985	1.55	4.32	CoMo-2
Solution-3		-	0.518	0.666	1.28	4.64	NiMo-1
Solution-4		-		0.951	1.83	3.91	NiMo-2

To study the precipitates formed directly in the impregnation solutions, “Solution-1” and “Solution-3” were divided into two parts. The first part of the solution was used for support impregnation. The second part of the solution was left in a closed beaker to prevent water evaporation. As a result, after several hours, a precipitate formed at the bottom of the beaker (Fig. S2). In the case of Ni-Mo solutions, the precipitate formed almost immediately after dissolution of AHM.

For the deposition of metals onto the support, the vacuum impregnation method was used. Support granules were placed in a Schlenk flask and then evacuated. Afterwards, excess solution was added to ensure that the entire volume of granules was completely immersed in the solution. For more complete adsorption of the citrate complexes, the support granules were kept in the impregnation solution for 20 minutes at 60 °C then the excess solution was drained off. The catalysts were dried at 110°C for 4 hours under an air flow. The precipitate formed during granule impregnation was separated from the solution on a glass filter with a pore size of 16–40 μm. For this purpose, the Schlenk flask was vigorously shaken and the liquid phase was quickly transferred onto the glass filter. The obtained precipitates were left to dry on the filter overnight. The nomenclature of all obtained samples is given in Table 2.

Table 2. Nomenclature of the samples

Samples	Description
CoMo-1	$CoMo/Al_2O_3$ catalyst prepared with precipitate formation on the granules from Solution-1
CoMo-2	$CoMo/Al_2O_3$ catalyst prepared without precipitate formation from Solution-2
CoMo-S1	Precipitate obtained from the CoMo-1 catalyst
CoMo-S2	Precipitate obtained from the Co-Mo impregnation solution without support impregnation
NiMo-1	$NiMo/Al_2O_3$ catalyst prepared with precipitate formation on the granules from Solution-3
NiMo-2	$NiMo/Al_2O_3$ catalyst prepared without precipitate formation from Solution-4
NiMo-S1	Precipitate obtained from the NiMo-1 catalyst
NiMo-S2	Precipitate obtained from the Ni-Mo impregnation solution without support impregnation

2.2 Characterization

The content of molybdenum, cobalt, and nickel in the catalysts and in the obtained precipitates was determined using inductively coupled plasma atomic emission spectroscopy (ICP-AES) on a Perkin Elmer Optima 4300 DV instrument.

The textural properties of the catalysts were determined by nitrogen adsorption-desorption using an ASAP 2400 instrument. All catalysts were pre-calcined at 500 °C for 2 hours. Prior to analysis, the samples were conditioned under a flow of N_2 at 150 °C for 2 hours. The specific surface area was calculated using the BET method from nitrogen adsorption in the relative pressure (P/P_0) range of 0.05–0.30. The total pore volume was determined from the amount of nitrogen adsorbed at a relative pressure close to unity ($P/P_0 = 0.995$), assuming that all accessible pores are filled with condensed nitrogen in the normal liquid state. The pore size distribution was calculated using the

Barrett-Joyner-Halenda (BJH) method from the desorption branch of the isotherm. The inaccuracy of the method is 5 %.

The Raman spectra were collected on a LabRAM HR Evolution microscope (Jobin Yvon) single stage spectrometer with a CCD Symphony detector with 2048 horizontal pixels. The laser power (633 nm line of He-Ne laser) at the sample was less than 0.1 mW. The laser beam was focused with a wide-angle 50× objective, and the spot size was 2 μm. The spectral resolution was 0.7 cm^{-1}.

Infrared spectra were measured in attenuated total reflectance (ATR) mode in the frequency range of 4000–350 cm^{-1} with a resolution of 4 cm^{-1} and accumulation of 40 scans on an ALPHA II Fourier transform IR spectrometer (BRUKER). PLATINUM-ATR attachment (BRUKER).

X-ray diffraction (XRD) experiments for catalysts before and after reaction were performed in the transmission mode using MoK_α radiation (λ = 0.70932 Å) on STOE STADI MP device (STOE) and detector MYTHEN2 1K. Measurements were made by scanning in the angles range of 4-35° with a step of 0.015° at 2θ.

Experiments to study the surface morphology were carried out on a dual-beam TESCAN SOLARIS FE-SEM scanning electron microscope (TESCAN) with an accelerating voltage of 20 kV in secondary electron mode. The instrument is equipped with an AztecLive energy-dispersive X-ray spectrometer (EDX) (Oxford Instruments) with a semiconductor Si detector having an energy resolution of 128 eV. For the experiments, cross-section polished sections of the granules were prepared with a specified flatness of 0.25 μm. The polished section embedded in epoxy resin was coated with a conductive carbon layer 10–20 nm thick.

Sufidation and testing of the catalysts were carried out in a fixed bed reactor. A 10 cm^3 portion of granular catalyst (3-7 mm) was loaded into the reactor (D = 16 mm, L = 1200 mm). The weight of the catalysts was calculated from their bulk density. The catalyst's granules with a length of 3-7 mm were diluted with silicon carbide (grain F80) to ensure uniform distribution in the reactor and to decrease the temperature gradient in the catalyst bed. The sulfidation procedure of the catalysts was carried out in downflow operation mode at 4.0 MPa, with a sulfidation feedstock flow of 1.5 h^{-1} and

a volumetric ratio of H_2/sulfidation feedstock of 400 Nm^3/m^3, and two temperature regimes: 240 °C for 8 h and 340 °C for 8 h. Straight-run gasoil (SRGO) with dimethyl sulfide (20 g DMDS per 1 L of SRGO) was used as the sulfidation feedstock. The sulfided catalysts were tested in the hydrotreating of straight-run gasoil (S = 3264 ppm, N = 112 ppm) under the following conditions: P = 4.0 MPa, volumetric H_2/SRGO ratio = 400 Nm^3/m^3, LHSV = 2.5 h^{-1}, T_1 = 340 °C, T_2 = 350 °C, T_3 = 360 ºC. Each temperature regime was maintained for 24 h. During the first 24 h the catalysts reached steady state. The process parameters for the testing of all catalysts are given in Table 3.

Table 3. Process parameters of the catalyst testing conditions

Conditions	Stage number			
	1[1]	2	3	4
Feed	SRGO			
T, ºC	340	340	350	360
LHSV, h^{-1}	2.5	2.5	2.5	2.5
P, MPa	4.0	4.0	4.0	4.0
H_2/feed, Nm^3/m^3	400	400	400	400
Stage time, h	24	24	24	24

[1] – catalyst running-in to reach a steady state

Then, liquid products were sampled for each regime. The residual sulfur and nitrogen contents in liquid samples were determined using an Xplorer-NS Analyzer (TE Instruments) by oxidative combustion with chemiluminescence and ultraviolet detection, according to ASTM D5762 and ASTM D4629 for total nitrogen content and ASTM D5453 for total sulfur content. The inaccuracy of analysis was ± 10 %.

The catalytic activity was evaluated using the apparent rate constant K_p ($ppm^{-0.4}$ h^{-1}) (Equation 1):

$$K_p = \frac{LHSV}{n-1}\left(\frac{1}{S^{n-1}} - \frac{1}{S_0^{n-1}}\right) \quad (1)$$

where *LHSV* is the liquid hourly space velocity (2.5 h^{-1}); n =1.4 is the reaction order for the given feed used here; S is the residual sulfur content in the product (ppm); S_0 is the sulfur content in the feed (3264 ppm). Due to the fact that the catalysts may contain different amounts of metals because of precipitate formation, it was decided to compare the reaction rate constants normalized by the molybdenum content in the catalyst (Equation 2), which was determined by normalizing K_p to the mass of Mo in the catalyst loaded into the reactor [22].

$$K = \frac{K_p}{g(Mo)/mL} \quad (2)$$

3. Results and discussion

3.1 Investigation of precipitates

The precipitates obtained during impregnation of γ-Al_2O_3 support granules and those formed directly in the impregnation solution were studied by XRD, Raman, and ATR-FTIR spectroscopy. The elemental analysis data are given in Table 4. CoMo-S1 and NiMo-S1 obtained upon contact of the impregnation solution with γ-Al_2O_3 granules were also analyzed for aluminum content. All precipitates were characterized by a high molybdenum content of 54.2-59.3 wt.% The S1 series samples contained aluminum (1.84–2.01 wt.%) and had lower Co and Ni contents compared to the S2 series. This was especially pronounced for CoMo-S1 where the cobalt content was 0.67 wt.%. The presence of aluminum in the precipitate clearly indicates partial dissolution of the support by the impregnation solution and the incorporation of Al^{3+} cations into the precipitate. For NiMo-S2, the Ni/Mo atomic ratio was 0.22, which is close to the theoretical value for Anderson HPC (1/6 ≈ 0.17). In the case of CoMo-S2, the high Co/Mo ratio of 0.36 may indicate the presence of other cobalt compounds.

Table 4. Results of elemental analysis of the precipitates

Samples	Mo, wt.%	Co, wt.%	Ni, wt.%	Al, wt.%	Co(Ni)/Mo
CoMo-S1	59,3	0,67	-	2.01	0.018
CoMo-S2	54.2	12.0	-	-	0.36
NiMo-S1	54.6	-	5.24	1,84	0.15
NiMo-S2	57.5	-	7.89	-	0.22

The X-ray diffraction patterns of CoMo-S1, CoMo-S2, NiMo-S1, and NiMo-S2 are shown in Figure 1 and Figs. S3–S4. All compounds exhibit a complex set of reflections with major maxima in the ranges of 4-9° 2θ and 11-16° 2θ.

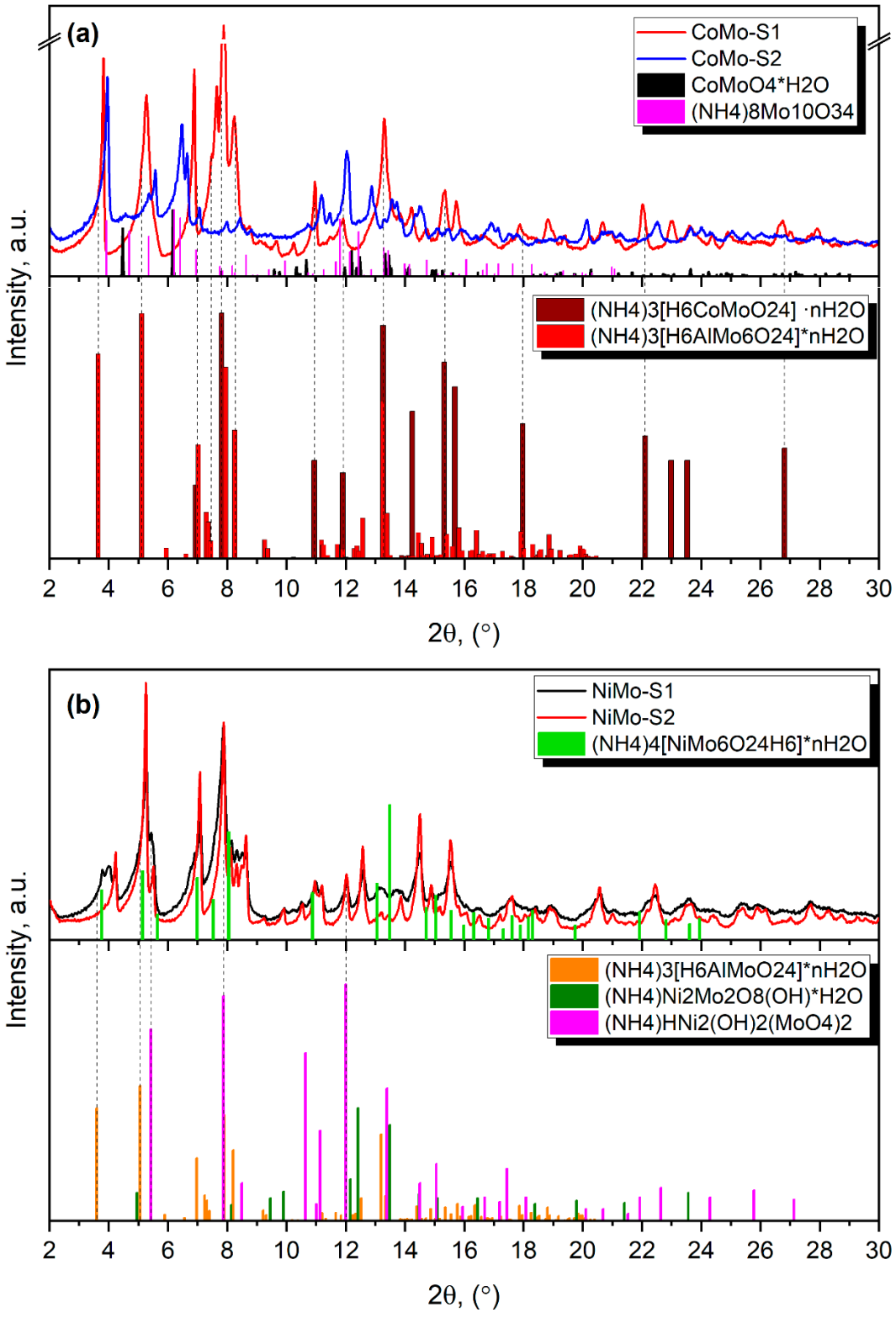


Figure 1. XRD patterns of the precipitates: (a) CoMo-S1 and CoMo-S2; (b) NiMo-S1 and NiMo-S2.

For the CoMo series, differences in the positions of several reflections are observed. A search of crystallographic databases shows that for CoMo-S1, the intense reflections at 3.8, 5.2, 7.8, 10.9, and 13.3° 2θ correspond to the HPCs $(NH_4)_3[AlMo_6O_{24}H_6]*nH_2O$ (PDF#04-013-4273) and $(NH_4)_4[CoMo_6O_{24}H_6]$ (PDF# 00-004-0226). For CoMo-S2, reflections at 3.9, 5.57, 6.5, 11.1, and 12.0° 2θ are pronounced and correspond to two compounds – $(NH_4)_8Mo_{10}O_{34}$ and $(NH_4)_2Mo_2O_7$. For NiMo-S1 and NiMo-S2, no significant differences are observed in the diffraction patterns and all major reflections correspond well to the compounds $(NH_4)_4[NiMo_6O_{24}H_6]*nH_2O$ (PDF#00-022-0506) and $(NH_4)_3[AlMo_6O_{24}H_6]*nH_2O$.

It is known that Raman spectroscopy is a powerful tool for studying the chemical and structural properties of inorganic materials that may be formed at various stages of catalyst preparation. A comparative study was performed for all four precipitates. The Raman spectroscopy data for CoMo-S1/S2 and NiMo-S1/S2 are shown in Figure 2. The spectrum of the CoMo-S1 sample (a) contains clear bands at 936, 892, 560, 352, and 211 cm^{-1}. The band at 936 and the weak shoulder at 920 cm^{-1} correspond to the stretching vibrations υ_s(Mo=O) in molybdenum ions with tetrahedral oxygen coordination and are characteristic of most molybdates. The band at 892 cm^{-1} is attributed to vibrations of bridging bonds υ(O–Mo_b–O). The band in the region of 560 cm^{-1} is characteristic of heteropolyanions (HPAs) with the Anderson structure $[X^{n+}M_6O_{24}H_6]^{6-n}$ and is assigned to the stretching vibrations of bridging bonds υ(Mo–O_c(X)–Mo) [23, 24], where X = Al^{3+}, Co^{2+}, Ni^{2+}, etc. In our case, the characteristic band at 560 cm^{-1} unambiguously indicates the HPC $(NH_4)_3[AlMo_6O_{24}H_6]*nH_2O$, where the central heteroatom is the Al^{3+} cation formed upon contact of $[MoO_4]^{2-}$ with γ-Al_2O_3 [19, 25, 26]. For the Co-containing HPC $(NH_4)_4[CoMo_6O_{24}H_6]$, the vibration band shifts to the low-frequency region around 540 cm^{-1} [27]. In the low-frequency region, deformation vibrations of bonds are observed: δ(O-Mo-O) at 352 cm^{-1} and δ(Mo-O_b-Mo) at 211 cm^{-1}. In contrast to CoMo-S1, for the CoMo-S2 sample, which formed in the solution without contact with the γ-Al_2O_3 support, a completely different pattern is observed. Firstly, the characteristic vibration in the 550-600 cm^{-1} region is absent indicating the absence of Anderson-type HPCs.

Secondly, in the 700-980 cm^{-1} a strong broadening of the main bands is observed. By deconvoluting the spectrum, vibrations at 716, 785, 860, 892, 915, and 936 cm^{-1} can be distinguished. This set of signals does not allow unambiguous identification of the compounds formed. Based on a number of literature data, they can be assigned to various polymolybdates [28–30]. According to XRD data, the main components of CoMo-S2 are $(NH_4)_8Mo_{10}O_{34}$ and $(NH_4)_2Mo_2O_7$. On the one hand, these data might be considered erroneous, since ammonium molybdates are to some extent soluble in water. On the other hand, a number of literature sources report studies on the preparation of certain crystalline ammonium molybdates in an aqueous medium. For example, reference [31] describes a method for obtaining $(NH_4)_8Mo_{10}O_{34}$, $(NH_4)_2Mo_2O_7$, and $(NH_4)_2Mo_4O_{13}$. In work [32], $(NH_4)_2Mo_2O_7$ was obtained by crystallization from an aqueous solution with a molybdenum concentration of at least 120 g/L. In our case, the molybdenum concentration in the impregnation solution was 1.59 mol/L, which corresponds to 152 g/L and exceeds the value reported in the literature. Therefore, in the absence of a sufficient amount of a chelating agent (citric acid) in concentrated impregnation solutions, crystallization of $(NH_4)_2Mo_2O_7$ can indeed be expected. However, a more likely compound is the sparingly soluble ammonium polyoctamolybdate $(NH_4)_{6n}(Mo_8O_{27})_n*nH_2O$, which forms in concentrated solutions of ammonium heptamolybdate [18, 33, 34]. A comparison of the Raman spectrum of ammonium polyoctamolybdate with that of CoMo-S2 is shown in Figure S5. In any case, the exact positions of the bands in the Raman spectra may differ from those described in the literature. This may be caused either by the incorporation of a heterocation into the structure of the molybdate anions or by symmetry distortion due to different degrees of hydration, protonation, or co-crystallization of several types of polymolybdates. In the case of the NiMo-S1 and NiMo-S2 samples, the Raman spectral signals are completely identical for both samples. The positions of the main bands correspond well to Anderson-type HPCs [17,35] and are attributed to $(NH_4)_4[NiMo_6O_{24}H_6]*nH_2O$. The aluminum present in NiMo-S1 according to ICP-AES data is most likely represented as the HPC $(NH_4)_3[AlMo_6O_{24}H_6]$. However, distinguishing its bands in the Raman spectrum is extremely difficult due to overlap with the bands of $(NH_4)_4[NiMo_6O_{24}H_6]*nH_2O$.

The formation of HPCs is confirmed by infrared spectroscopy. The FTIR spectra of all samples are shown in Figure 3. The characteristic absorption bands of CoMo-S1, NiMo-S1, and NiMo-S2 coincide with those of Anderson HPCs described in the literature [26,27,36,37]. The IR spectrum of XMo_6 is typical of the heteropolyanion arrangement: *cis*-(MoO_{2t}) terminal stretching at 930, 900, and 870 cm^{-1}, ν(Mo-O-Mo) at 650 cm^{-1}, ν(X-O), (where X= Co, Ni or Al) ~ 575 cm^{-1}, ν(Mo-O_c-X) at 450 cm^{-1}, and δ(Mo-O, X-O) at ~380 cm^{-1}. For CoMo-S1, strongly pronounced absorption at 450 cm^{-1} is characteristic caused by distortion of the central heterocation. In the case of CoMo-S2, as in the Raman spectrum, a broad absorption region with broadened maxima at 856, 690, and 600 cm^{-1} is observed. This set of absorption bands is characteristic of polymolybdate structures, which exhibit many nonequivalent bridging Mo–O–Mo [38, 39].

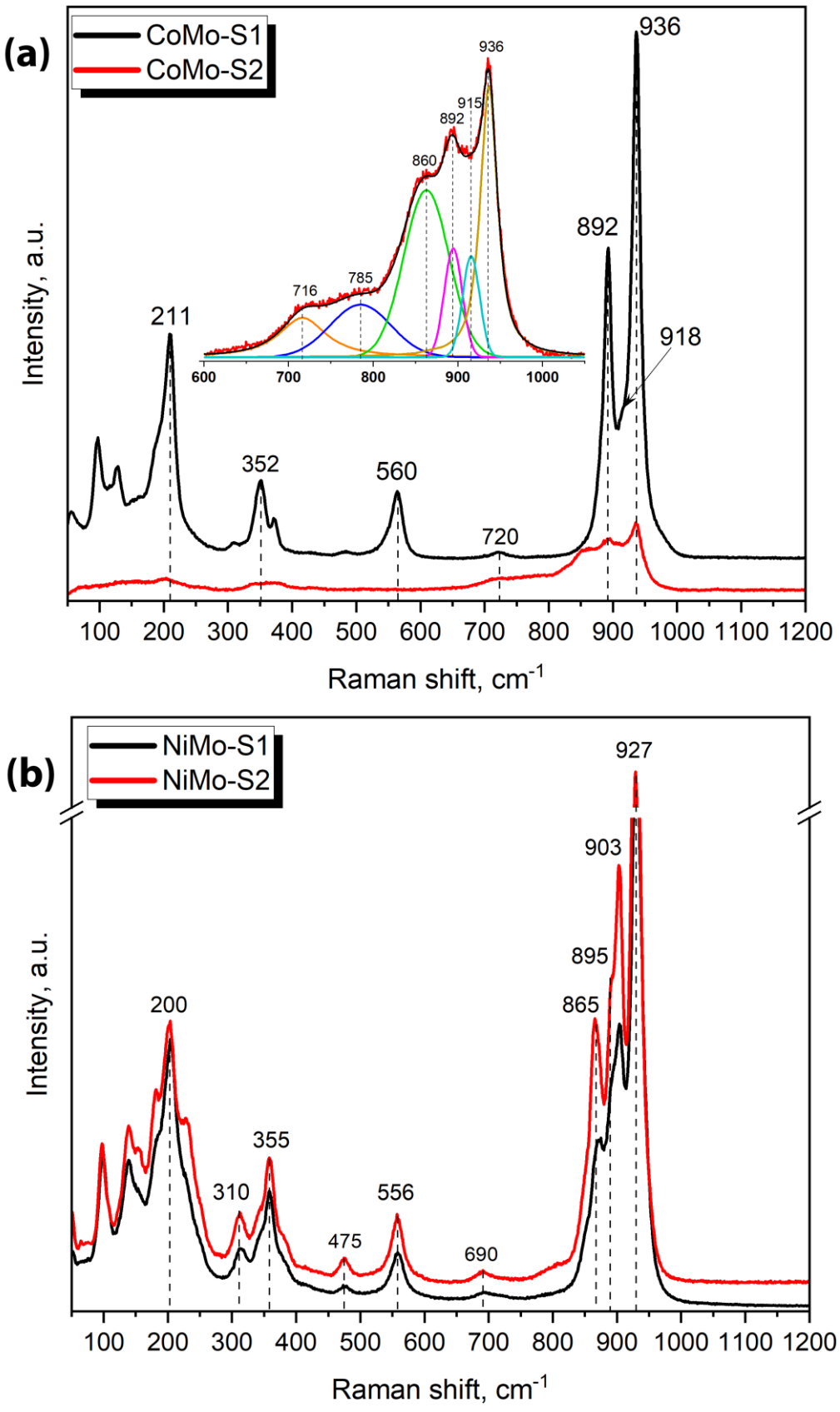


Figure 2. Raman spectra of (a) CoMo-S1/S2 and (b) NiMo-S1/S2 samples

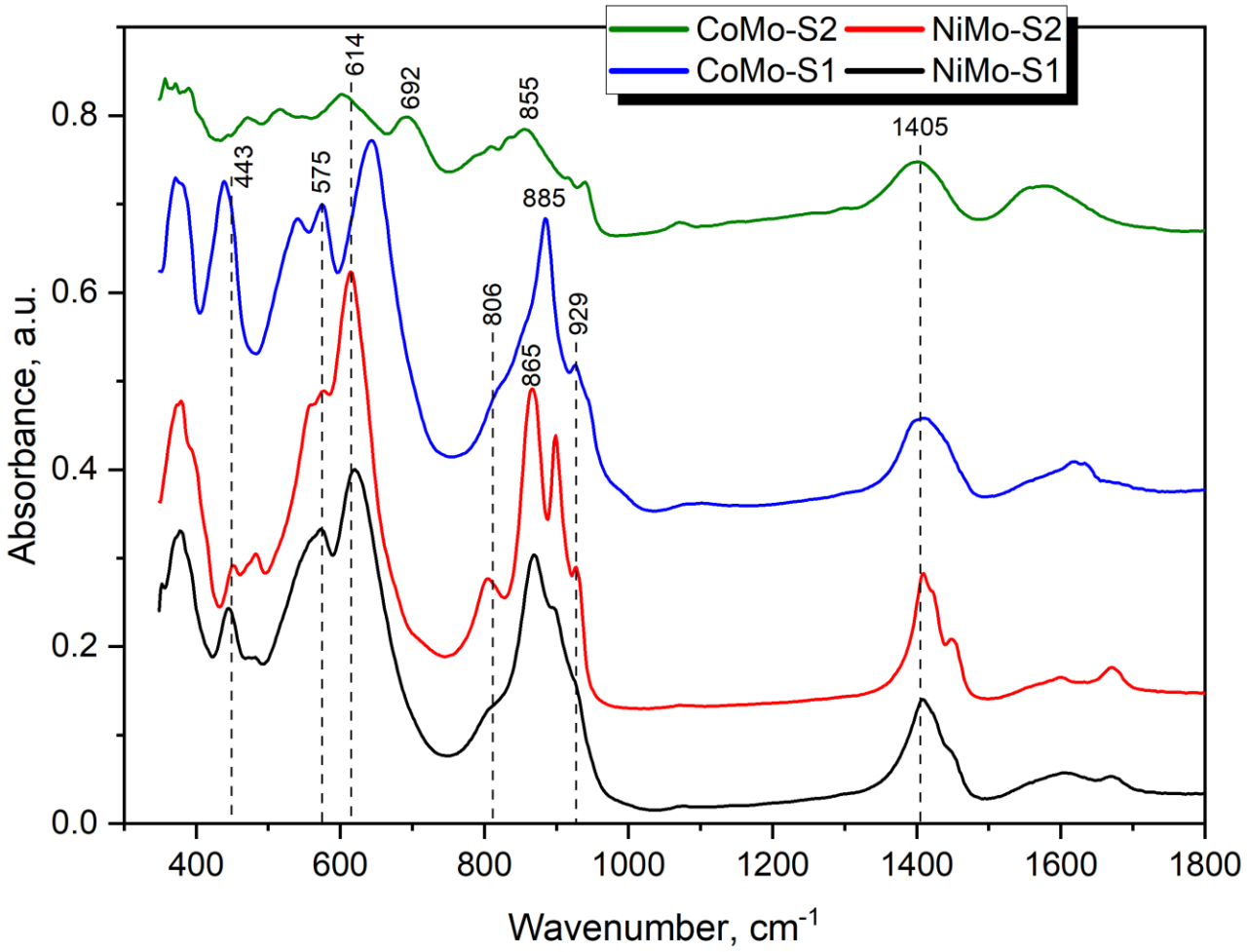


Figure 3. ATR-FTIR spectra of the CoMo-S1, CoMo-S2, NiMo-S1 and NiMo-S2

3.2 Investigation of the catalysts

3.2.1 Non-sulfided catalysts

Table 4 presents the elemental composition of the supported CoMo and NiMo series catalysts. The content of supported metals in the samples varies in the range of 9.38–11.0 wt.% for Mo, 2.67–3.28 wt.% for Co, and 2.56–2.79 wt.% for Ni. All investigated catalysts are characterized by high values of the promoter-to-molybdenum atomic ratio (Co(Ni)/Mo), which exceed the calculated values (0.4

for CoMo and 0.33 for NiMo). In the CoMo series, this ratio is 0.46 and 0.48; in the NiMo series, it is 0.40 and 0.41. The samples that were in contact with precipitates (CoMo-1 and NiMo-1) exhibit higher concentrations of active metals. This is a direct consequence of the deposition of precipitate particles containing active metals onto the surface of the catalyst granules.

Table 4. Results of elemental analysis of the catalysts

Samples	Mo, wt.%	Co, wt.%	Ni, wt.%	Co(Ni)/Mo
CoMo-1	11.0	3.28	-	0.48
CoMo-2	9.38	2.67	-	0.46
NiMo-1	11.0	-	2.79	0.41
NiMo-2	10.3	-	2.56	0.40

The phase composition of the catalysts was studied by X-ray powder diffraction. In the diffraction patterns of both samples, reflections characteristic of the metastable low-temperature form γ-Al_2O_3 (PDF#00-029-0063) are observed (Figure 4). The determined lattice parameter was a=7.919(2)Å. The average crystallite size D_{XRD} was 5.5 nm. The presence of an additional peak at 19.2° 2θ (d/n=2.12 Å) indicates the presence of the low-temperature metastable χ-Al_2O_3 form. In the diffraction pattern of the CoMo-1 sample, reflections characteristic of the crystalline phases $(NH_4)_4[H_6CoMo_6O_{24}]*nH_2O$ (PDF# 00-004-0226) and $(NH_4)_3[AlMo_6O_{24}H_6]*nH_2O$ (PDF#04-013-4273) are also observed. The average crystallite size of these phases was D_{XRD}~12-13 nm. In the diffraction pattern of the NiMo-1 sample (Figure 5), peaks whose positions and relative intensities are characteristic of the phases $(NH_4)_3[AlMo_6O_{24}H_6]*nH_2O$ (PDF# 04-013-4273) and $(NH_4)_4[H_6NiMo_6O_{24}]*nH_2O$ (PDF# 00-022-0506) are observed, with an average crystallite size of D_{XRD}~8-10 nm. For NiMo-2, as well as for CoMo-2, only reflections of γ-Al_2O_3 are characteristic.

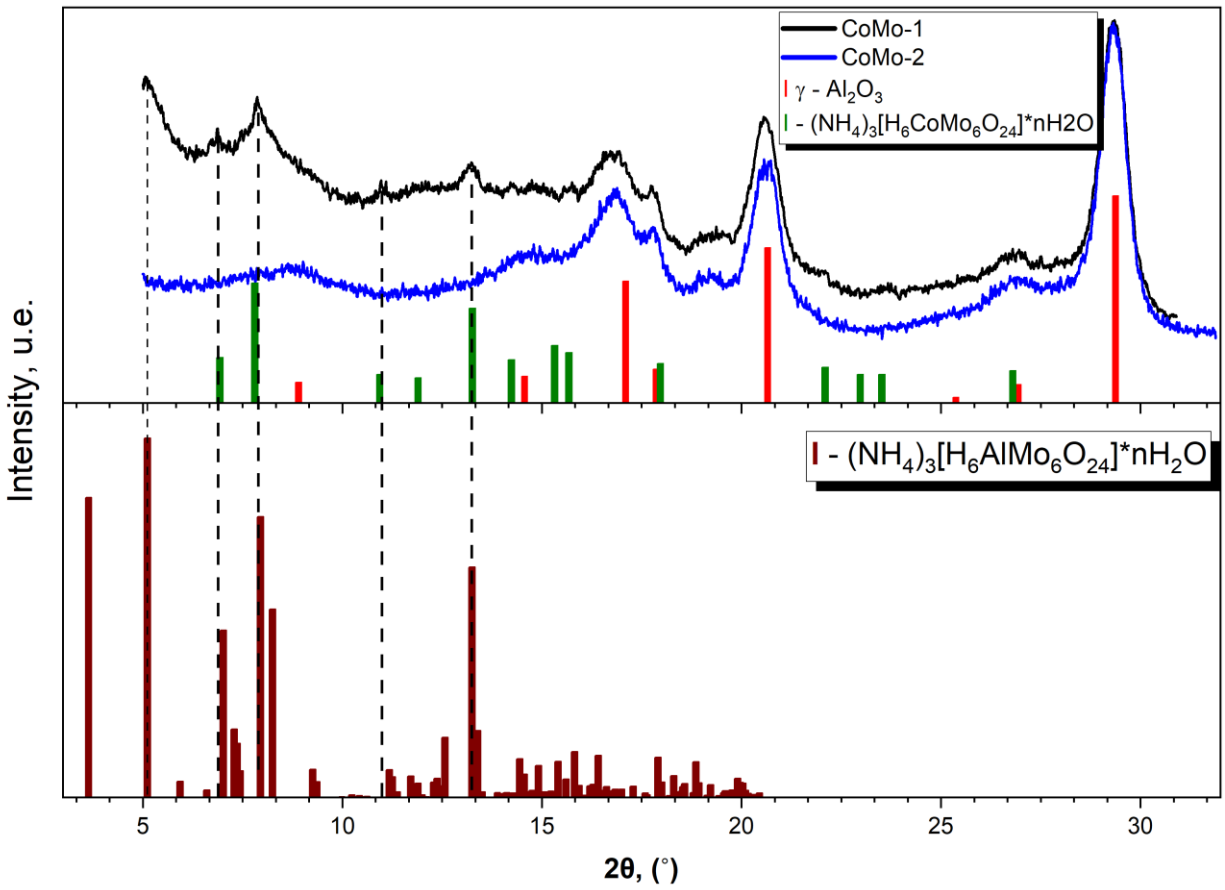


Figure 4. XRD patterns of the CoMo-1 and CoMo-2 catalysts

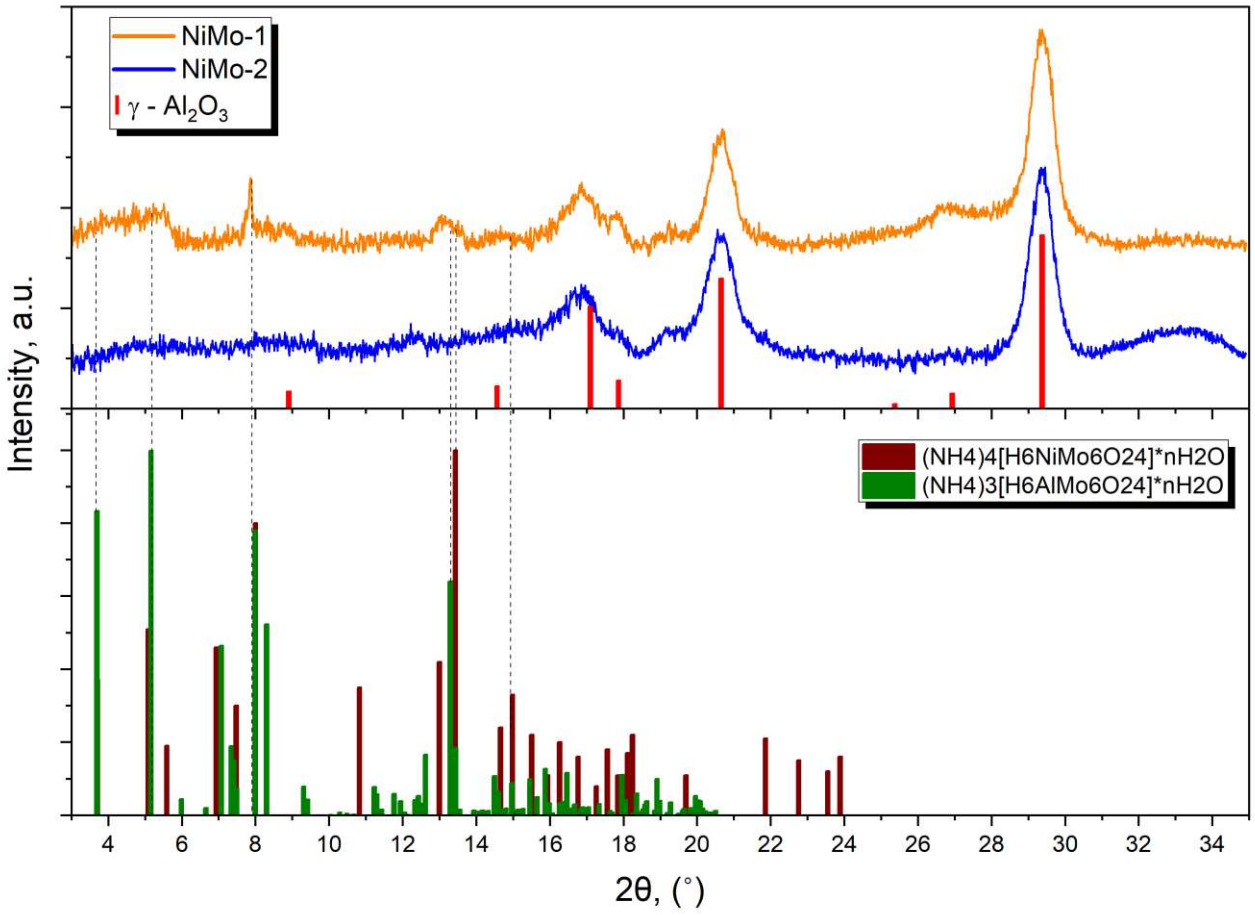


Figure 5. XRD patterns of the NiMo-1 and NiMo-2 catalysts

For more precise identification of the compounds formed on the surface of the CoMo-1 and NiMo-1 catalyst granules, Raman microspectroscopy was used. Raman microspectroscopy combines Raman spectroscopy with an optical microscope, providing non-destructive point analysis of microscopic samples. The data for CoMo-1 and NiMo-1 are shown in Figures 6 and 7. Both catalysts are characterized by the presence of crystalline formations on the granule surface. The positions of the main vibrational bands in the Raman spectra of these crystallites indicate the presence of HPCs. For CoMo-1, the main vibrational bands at 650, 900, and 570 cm^{-1} unambiguously indicate the presence of the HPC $(NH_4)_4[CoMo_6O_{24}H_6]$ *nH_2O [40]. For $(NH_4)_4[NiMo_6O_{24}H_6]$ *nH_2O, the main bands are at 945, 914, and 567 cm^{-1} [17]. Regarding $(NH_4)_3[AlMo_6O_{24}H_6]$, this HPC is isostructural with respect to $(NH_4)_4[CoMo_6O_{24}H_6]$ *nH_2O and $(NH_4)_4[NiMo_6O_{24}H_6]$ *nH_2O [19,24], and it is not possible to distinguish its individual vibrations.

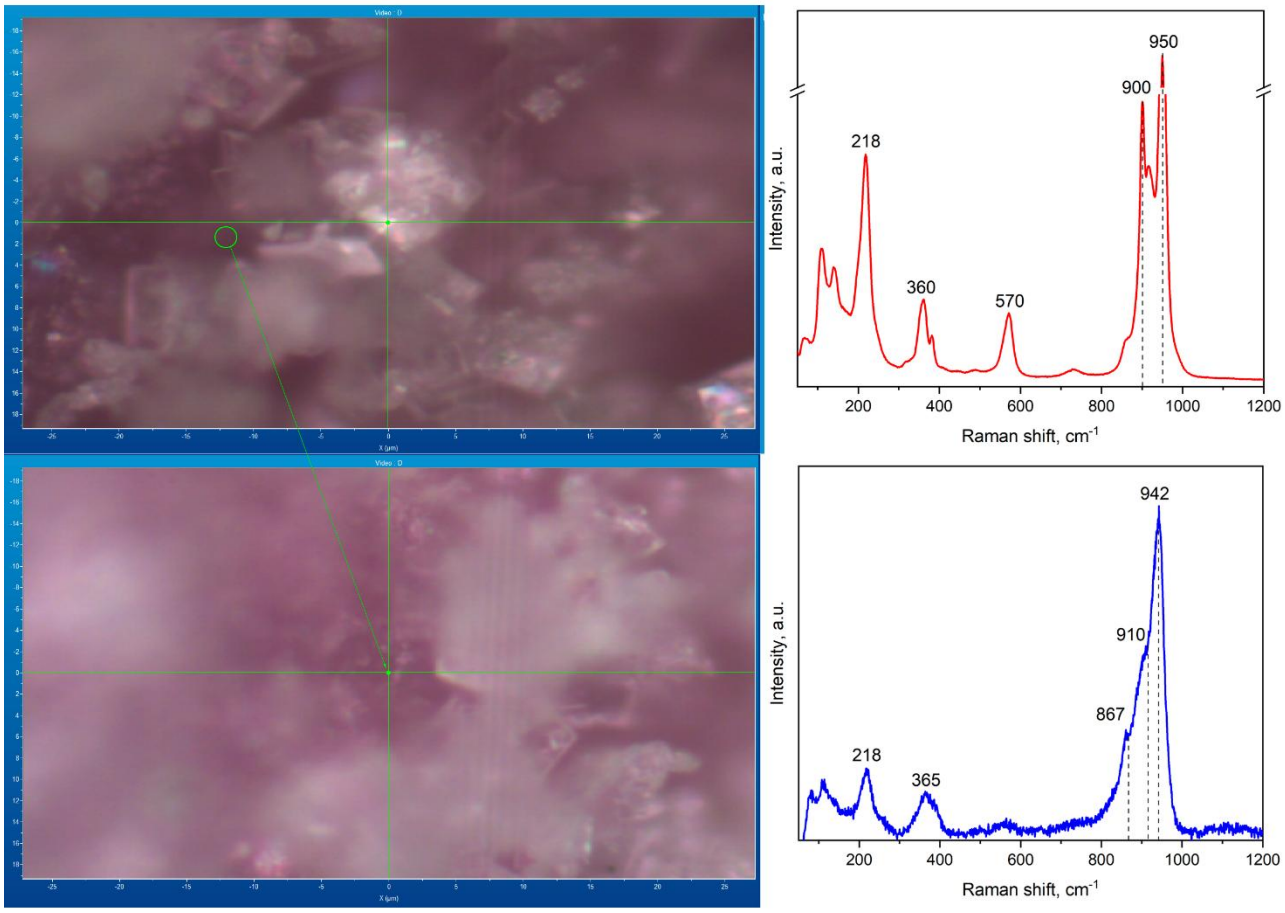


Figure 6. Raman microspectroscopy of CoMo-1. Image of an HPC crystal $(NH_4)_4[CoMo_6O_{24}H_6]$ and its Raman spectrum (top). Catalyst region free of $(NH_4)_4[CoMo_6O_{24}H_6]$ and its Raman spectrum (bottom).

Analysis of the surface of CoMo-1 and NiMo-1 catalyst granules free of HPC crystallites shows that the main compound is the citrate complex anion $[Mo_4O_{11}(Citr)_2]^{2-}$ [10,20,41]. A weak reflection at ~ 560 cm^{-1} may indicate the joint presence of minor amounts of HPCs together with the citrate complexes.

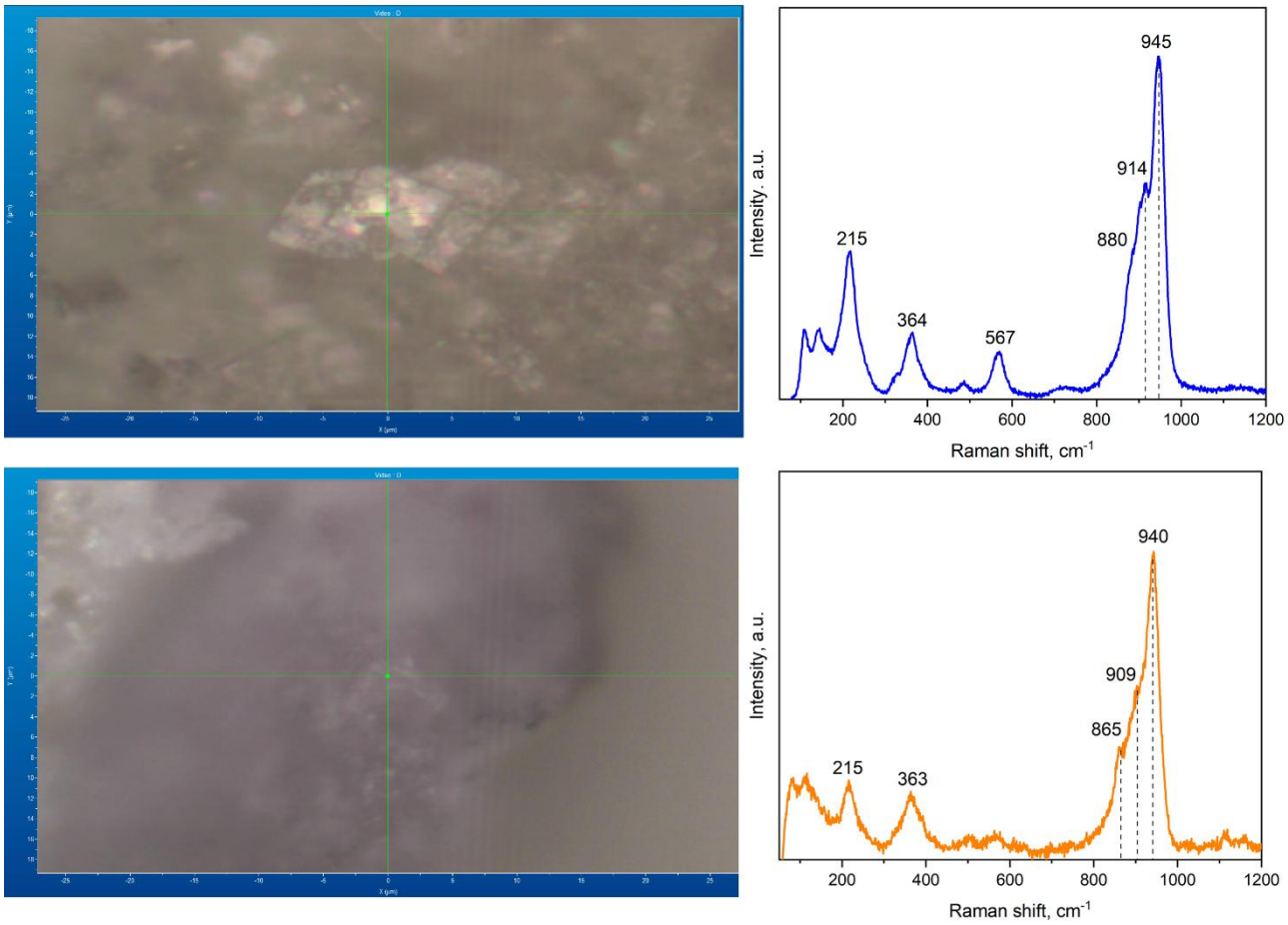


Figure 7. Raman microspectroscopy of NiMo-1. Image of an HPC crystal of $(NH_4)_4[NiMo_6O_{24}H_6]$ and its Raman spectrum (top). Catalyst region free of HPCs $(NH_4)_4[NiMo_6O_{24}H_6]$ and its Raman spectrum (bottom).

The distribution and morphology of the active metals and the deposition of their compounds on the surface of the catalyst granules were studied by scanning electron microscopy (SEM). For the CoMo-1 catalysts, the formation of bulk crystalline agglomerates with a size of 0.1–1 mm is characteristic on the granule surface (Figure 8). Upon closer examination of individual areas of the catalyst, it is found that the accumulation of agglomerate particles occurs predominantly in the geometric depressions of the trilobe granule (Figure S6).

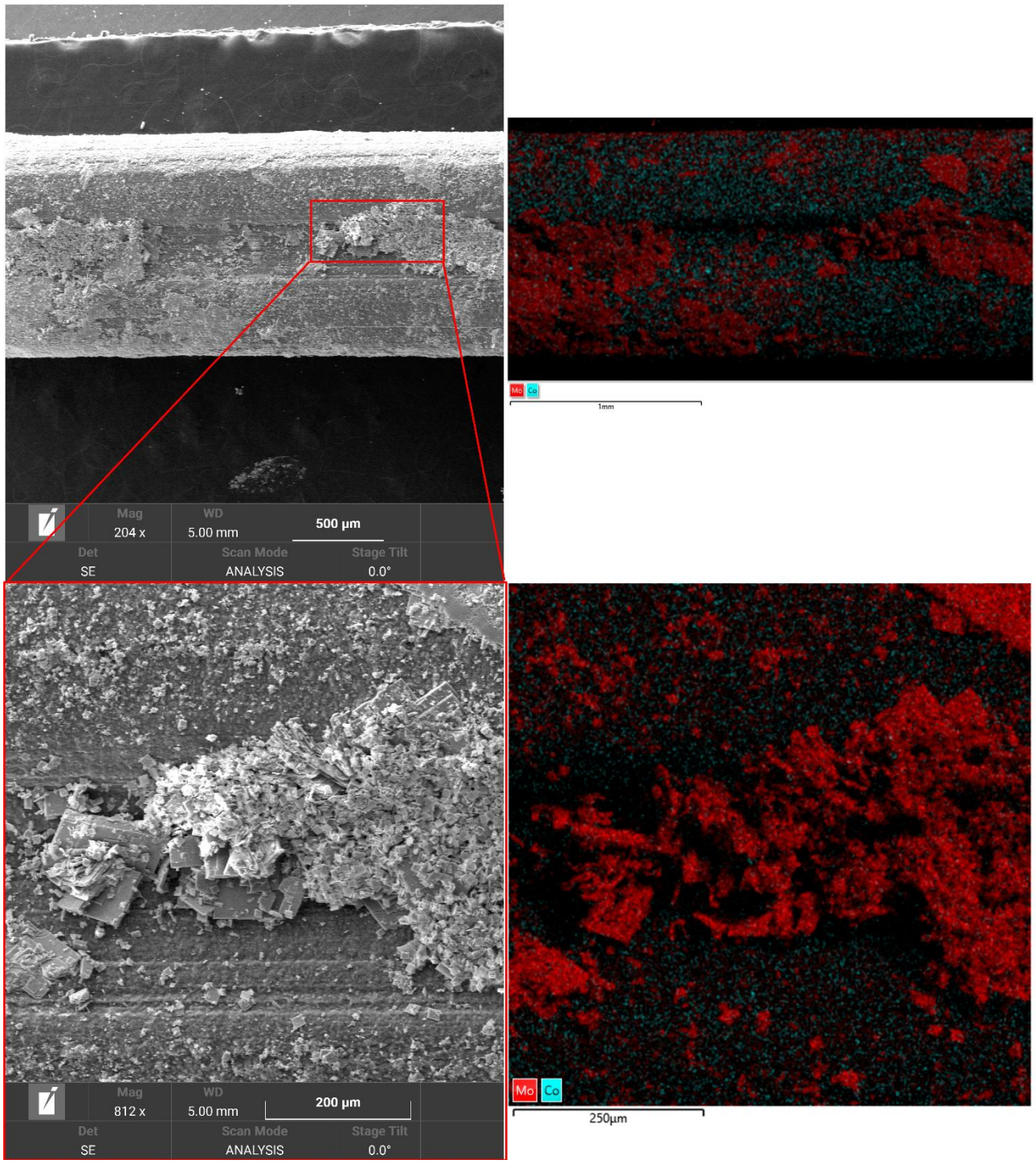


Figure 8. SEM-EDX images of the surface of the CoMo-1 catalyst

The CoMo-2 sample is characterized by a uniform distribution of active metals over the granule surface and the absence of large agglomerates (Figure 9). Only isolated particles smaller than 50 µm can be noted. In all cases, for both CoMo-1 and CoMo-2, a uniform distribution of cobalt and molybdenum across the granule cross-section was observed.

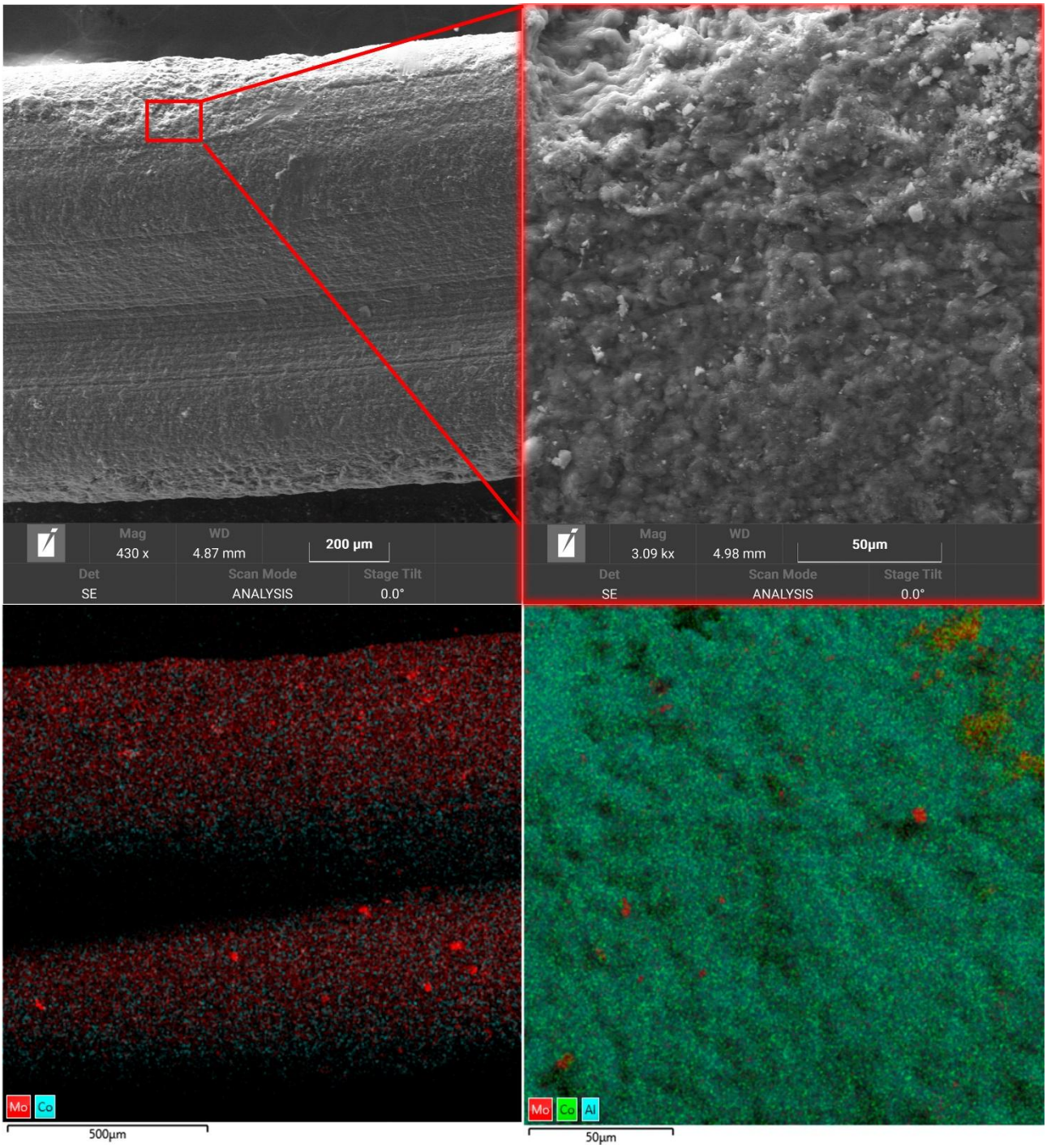


Figure 9. SEM-EDX images of the surface of the CoMo-2 catalyst

In the case of the NiMo-1 catalyst, the deposits on the granule surface are represented by rhombic crystalline particles with a size of 20–30 µm, which form clusters up to ~100 µm in size (Figure 10). For NiMo-2, as well as for CoMo-2, a uniform distribution of metals over the granule surface without the formation of any individual particles is characteristic (Figures S7, S8).

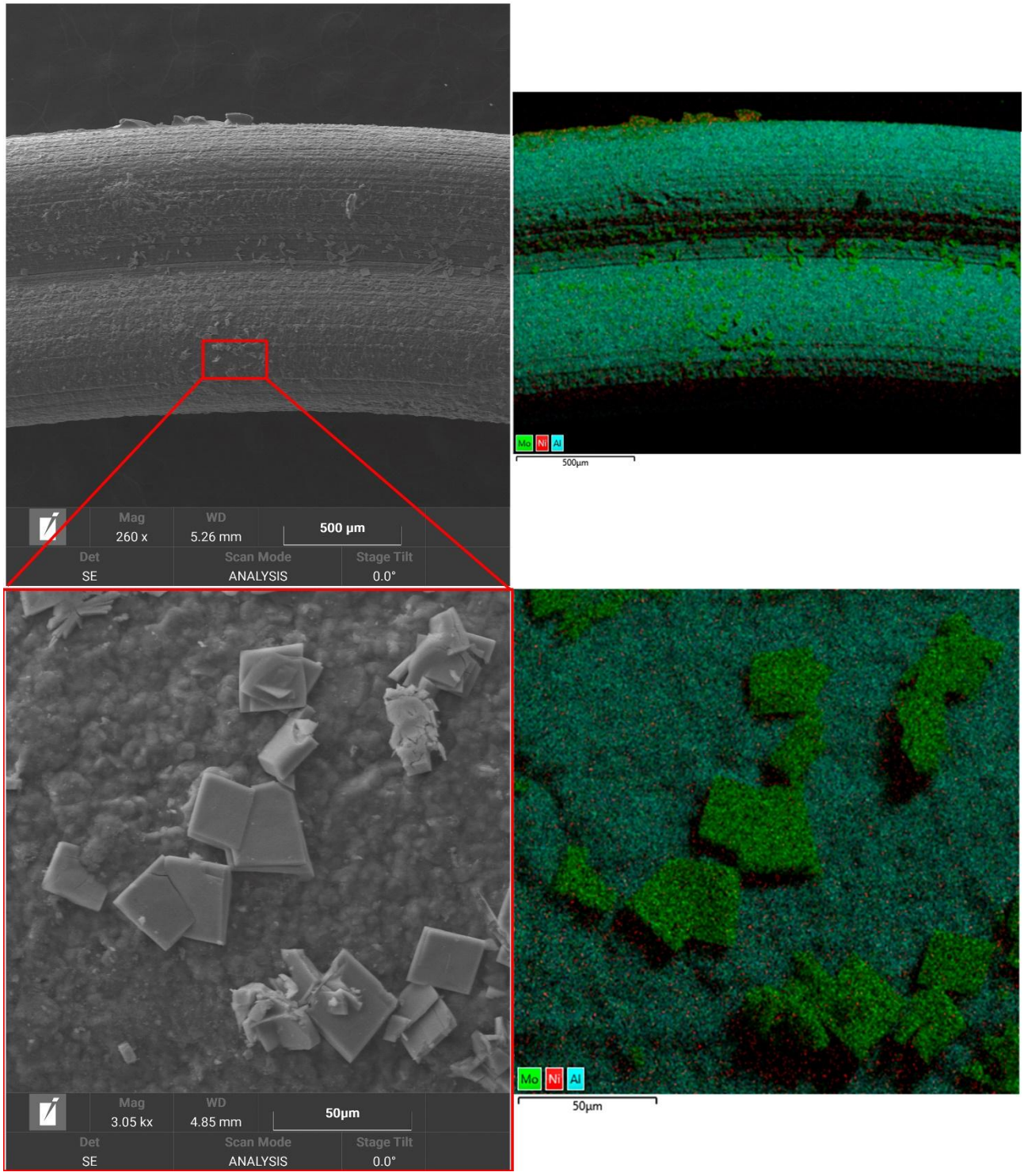


Figure 10. SEM-EDX images of the surface of the NiMo-1 catalyst

Summarizing the obtained data, assumptions about the mechanism of precipitate formation can be made. It is known that during the joint dissolution of AHM and Co(Ni) salts in a citric acid solution, a complex compound $[M(H_2O)_x]_2[Mo_4O_{11}(Cit)_2]$ is formed, where M = Co^{2+} or Ni^{2+}, and the ammonium ion originating from AHM binds with NO_3^- or CH_3COO^-, forming NH_4NO_3 or

CH_3COONH_4 respectively [41, 42]. A similar study for solutions obtained by dissolving Ni(Co) hydroxides and AHM in citric acid is currently absent. Obviously, in such solutions, citric acid not only forms complex citrates with active metals but also binds the ammonium ion. The formation of ammonium citrate can be considered as a competitive complexation reaction with $[MoO_4]^{2-}$ anions. From a thermodynamic point of view, the formation of HPCs is more favorable compared to citrate complexes. The cooperative binding of six MoO_6 octahedra around a central heteroatom – Co, Ni, and Al – creates a more favorable energy minimum than coordination with the carboxyl groups of the citrate ion. In contrast to HPCs, citrate complexes are stabilized primarily by the chelate effect of carboxyl groups, which provides a smaller energy gain. Thus, the equilibrium constant values (pK) for $(NH_4)_4[NiMo_6O_{24}H_6]$ and $[MoO_4H_2Cit]^{3-}$ are 44.3 and 18.1, respectively [43]. Consequently, when citric acid is deficient, the predominant form in the solution will be ammonium citrate, whose chelating effect is even less pronounced than that of citric acid itself. This leads to a decrease in the stability of the citrate complex $[Mo_4O_{11}(Cit)_2]^{4-}$ and the appearance of free $[MoO_4]^{2-}$ anions. The $[MoO_4]^{2-}$ anions formed in the solution undergo chemical reactions with Ni^{2+}, Co^{2+}, or Al^{3+} cations to form HPAs $[X^{n+}Mo_6O_{24}H_6]^{6-n}$. The HPAs in turn bind with ammonium ions, forming sparingly soluble ammonium salts $(NH_4)_{6-n}[X^{n+}Mo_6O_{24}H_6]$ (Eq. 1-3).

$$7[MoO_4]^{2-} + 8H^+ \leftrightarrow [Mo_7O_{24}]^{6-} + 4H_2O \quad (1)$$

$$6[Mo_7O_{24}]^{6-} + 7X^{n+} + 24H_2O \rightarrow 7[X^{n+}Mo_6O_{24}H_6]^{6-n} + 6H^+, \quad \text{where } X = Co^{2+}, Ni^{2+}, \text{ or } Al^{3+} \quad (2)$$

$$[X^{n+}Mo_6O_{24}H_6]^{6-n} + 6\text{-}nNH_4^+ \rightarrow (NH_4)_{6-n}[X^{n+}Mo_6O_{24}H_6] \downarrow \quad (3)$$

HPAs featuring a transition metal central heteroatom tend to undergo substitution by lighter elements. Thus, the contact of $(NH_4)_4[Co(Ni)Mo_6O_{24}H_6]$ *nH_2O with the support involves its surface Al atoms, leading to the formation of $(NH_4)_3[AlMo_6O_{24}H_6]$ *nH_2O (Eq. 4) [36,44].

$$(NH_4)_{6-n}[X^{n+}Mo_6O_{24}H_6] + Al_2O_3 \rightarrow (NH_4)_x[X_{3-x/n}AlMo_6O_{24}H_6]/Al_2O_3 + X\text{-}Al\text{-}O \quad (4)$$

where X = Co^{2+}, Ni^{2+}

In the case of Co-Mo citrate solutions that are not in contact with alumina, the main route of precipitate formation proceeds through the formation of polymolybdates. This fact is most likely due to the specific features of Co^{2+} complexation process. It should also be taken into account that the Al_2O_3 support can locally increase the pH of the impregnation solution (Point of Zero Charge (PZC) ~ 8) and influence the structure and local distribution of molybdenum complexes [45, 46]. The above assumptions may not be entirely correct. Nevertheless, they help explain the formation of precipitates and require further, more detailed studies of the state of metal ions in citrate solutions.

3.2.2 Sulfided catalysts

Figure 11 shows Co2p and Ni2p spectra of the sulfided catalysts. The presented spectra are normalized to the Al2p line intensity of the corresponding samples. Two peaks are present in the spectra with binding energies of ~778.7 eV and ~781.2 eV. The peak with a $Co2p_{3/2}$ binding energy of ~ 778.7 eV is characteristic of Co^{2+} in the CoMoS phase [47, 48]. The peak at ~781.2 eV corresponds to cobalt in the mixed oxide Co_3O_4, however, for these samples distinguishing between the peaks corresponding to Co^{2+} and Co^{3+} states is difficult. Two peaks with binding energies of ~853.5 eV and ~856.6 eV are characteristic of Ni^{2+} in the NiMoS phase [47, 49] and in NiO [50], respectively. The remaining peaks, shifted to higher binding energies, are shake-up satellites characteristic of Co^{2+} and Ni^{2+}. The Mo3d and S2p spectra of the sulfided catalysts are shown in Figure S9. Mo3d spectra for all samples are represented as two doublets with binding energies of $Mo3d_{5/2}$ at ~ 228.8±0.1 eV, characteristic of molybdenum in the Mo^{4+} state, and $Mo3d_{5/2}$ at ~ 232.2±0.1 eV, corresponding to the Mo^{6+} state. The spectra of the CoMo-1, NiMo-1, and NiMo-2 samples are described by two doublets with $S2p_{3/2}$ binding energies of ~ 161.6 eV, attributed to sulfur in the sulfide form S^{2-}, and at ~ 168.7 eV $S2p_{3/2}$, characteristic of sulfate sulfur S^{6+}. Additionally, for the CoMo-2 sample, a doublet with an $S2p_{3/2}$ binding energy of ~ 163.3 eV is observed, characteristic of sulfide sulfur S^{2-} in MoS_2 [50]. The atomic surface ratios of the elements and the fractions of different states for the studied elements are given in Table 5. For the CoMo-1 and CoMo-2 samples,

the quite close atomic ratios Co/Mo, Co/S, Mo/S, and S/Al are noteworthy, allowing the conclusion that the surface composition is similar for the samples with and without precipitate. The NiMo-1 and NiMo-2 samples differ somewhat more noticeably. The sample with the precipitate is characterized by a slightly lower content of Ni^{2+} in the NiMoS phase and a higher content of sulfate sulfur. The formation of sulfates on the catalyst surface is likely related to exposure of the samples to the atmosphere during sample preparation prior to XPS analysis. As can be seen from Table 5, the cobalt-based catalysts are characterized by a similar fraction of the Co-Mo-S phase, which is about 55 at.%. For the Ni-containing catalysts, the fraction of the NiMoS phase is also similar and amounts to about 70 at.%. Thus, from the XPS data it can be concluded that the formation of a precipitate during catalyst preparation does not lead to a significant change in the surface composition of the catalysts. Thus, from the XPS data it can be concluded that the formation of a precipitate during catalyst preparation does not lead to a significant change in the surface composition of the catalysts.

The distribution of active metals on the surface of catalyst granules in the sulfide state after catalytic testing was studied by SEM-EDX. Visual evaluation of the images showed that the surface of catalyst granules on which HPCs had formed (NiMo-1 and CoMo-1) has a non-uniform structure and exhibits a crust-like coating of MoS_2 sulfide particles (Figures. 12 and S10). Images of the catalysts at a resolution of 10 μm show that MoS_2 particles are irregular polygons. Mapping revealed that the surface of the irregular MoS_2 polyhedra contains uniformly distributed molybdenum and sulfur atoms. CoMo-2 is characterized by the absence of sulfide particles on the granule surface.

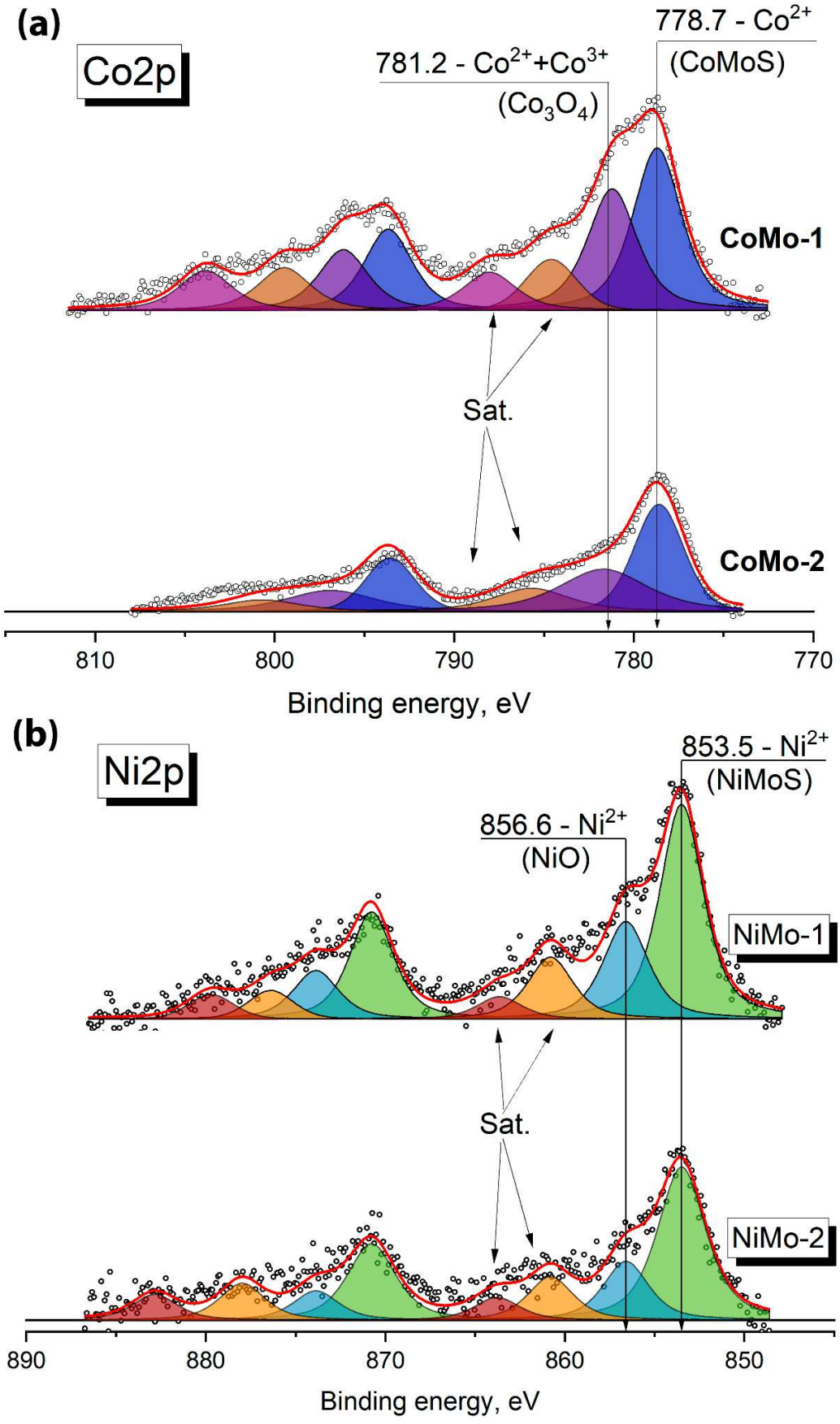


Figure 11. Co2p (a) and Ni2p (b) spectra of the catalysts

Table 5. XPS data of catalysts

Samples	CoMo-1	CoMo-2	NiMo-1	NiMo-2
The atomic ratio of elements on the surface				
Co/Mo	0.62	0.59	-	-
Ni/Mo	-	-	0.30	0.37
Co/S	0.36	0.31	-	-
Ni/S	-	-	0.16	0.21
Mo/S	0.59	0.52	0.53	0.56
S/Al	0.18	0.20	0.25	0.15
Surface content of elements in different states, at. %				
Mo^{4+}	97	89	97	94
Mo^{6+}	3.5	11	2.7	6.0
Co^{CoMoS}	56	55	-	-
Co^{oxide}	44.0	67.4	-	-
Ni^{NiMoS}	-	-	68	73
Ni^{oxide}	-	-	32	27
S^{2-}	93	90	89	87
S^{2+}	7.3	10	11	13

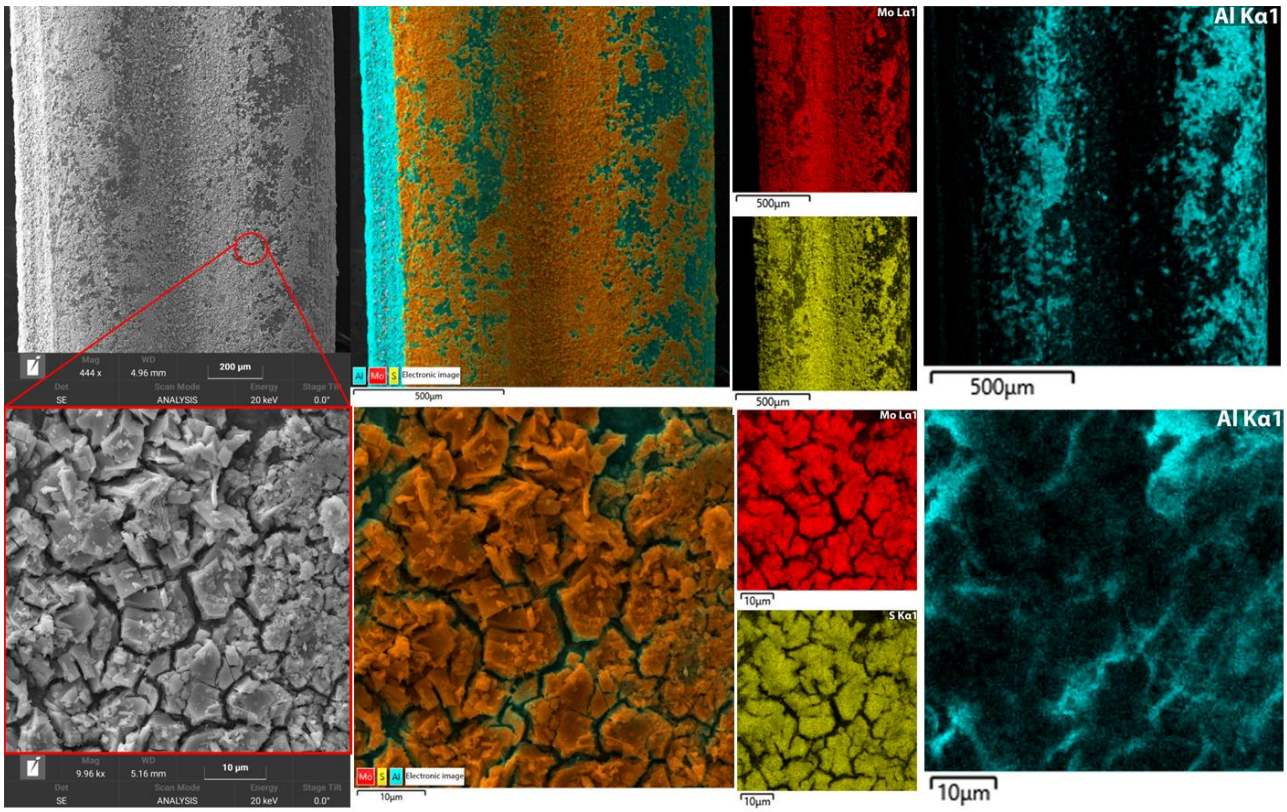


Figure 12. SEM-EDX images of the surface of the sulfided NiMo-1 catalyst

3.3 Catalytic activity

The residual sulfur and nitrogen contents in the hydrodesulfurization products of SRGO at different temperatures are given in Table 6 and Figure 13. The test conditions are comparable to the operating conditions of industrial low pressure gas oil hydrotreating units at most oil refineries worldwide. In each case, the rate constant values and the residual sulfur content are indicated.

Table 6. Residual sulfur and nitrogen content in the hydrotreated product

	Residual S content, ppm			Residual N content, ppm		
	340, °C	350, °C	360, °C	340, °C	350, °C	360, °C
CoMo-1	61	38	18	38	36	29
CoMo-2	57	50	24	38	33	23
NiMo-1	66	40	22	43	37	30

NiMo-2	69	40	23	37	31	24

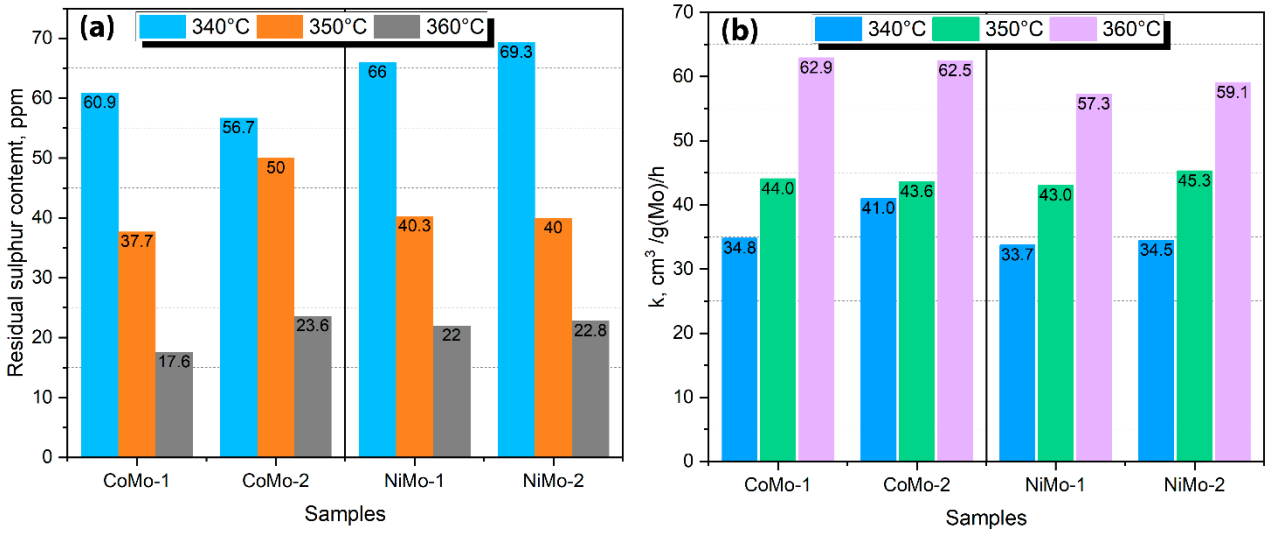


Figure 13. Residual sulfur content (a) and HDS rate constant (b).

The results of catalytic tests indicate that HPCs precipitation during impregnation does not impair catalyst activity. However, the observed differences in activity should be interpreted primarily in terms of the actual amount of active metals deposited as HPCs within the pores and on the surface of the support granules. The deposited HPCs particles - $[CoMo_6O_{24}H_6]^{4-}$, $[NiMo_6O_{24}H_6]^{4-}$, and their derivatives - are not catalytically inert. Anderson-type HPCs and related compounds have been widely investigated as precursors to the sulfide phase of hydrotreating catalysts. During sulfidation, these HPCs are converted into active type II Co(Ni)-Mo-S-phase particles [40, 44, 51–55]. Indeed, elemental analysis confirmed that catalysts prepared under precipitation conditions contained higher amounts of active metals. In the CoMo series, CoMo-1 contained 11.0 wt.% Mo and 3.28 wt.% Co, whereas CoMo-2 contained 9.38 wt.% Mo and 2.67 wt.% Co. A similar trend was observed for the NiMo catalysts, with NiMo-1 containing 11.0 wt% Mo and 2.79 wt% Ni, compared with 10.3 wt.% Mo and 2.56 wt.% Ni for NiMo-2. Thus, precipitation of heteropoly compound particles increased active metal loading.

This difference in active metal content is reflected in the catalytic activity data. In the CoMo series, CoMo-1 shows a lower residual sulfur content than CoMo-2 at 350 and 360 °C. At 360 °C,

the residual sulfur content decreases from 24 ppm for CoMo-2 to 18 ppm for CoMo-1. The higher catalytic activity of CoMo-1 can be attributed to its higher active metal content, which results from the deposition of heteropoly compounds (HPCs). In the NiMo series, the catalytic activities of NiMo-1 and NiMo-2 are comparable over the entire temperature range. The residual sulfur content is virtually identical at 350 and 360 °C, indicating that the increased Ni and Mo content in NiMo-1 does not produce a noticeable increase in activity. This may suggest that in NiMo-1, the additional active metals introduced via HPCs particle deposition contribute only partially to the formation of an accessible sulfidic Ni–Mo–S phase, while primarily compensating for diffusion or morphological limitations arising from the rapid and nonuniform deposition of the HPCs precipitate.

The results demonstrate that the formation of HPCs precipitates leads to additional deposition of active metals on the support and that, under sulfidation conditions, these particles can be converted into catalytically active sulfide phases, as confirmed by XPS and SEM–EDX data. Consequently, catalysts prepared under conditions involving precipitate formation retain - and, in the case of CoMo, even exceed - the activity of catalysts prepared from stable citrate-based impregnation solutions. From a practical standpoint, these findings indicate that the incidental formation of HPCs precipitates during industrial catalyst preparation does not necessarily justify product rejection. Nevertheless, the nonuniform distribution of HPCs and the resulting formation of sulfide particles should still be considered undesirable in catalyst manufacturing. Thus, stabilization of impregnation solutions with citric acid remains essential, not because the precipitate itself is catalytically inactive, but because preventing HPC precipitation enables better control over metal loading, the distribution of the active component within the support pore structure, and the reproducibility of catalyst properties.

Conclusion

The composition of precipitates formed both in citrate NiMo and CoMo impregnation solutions and upon contact of the impregnation solutions with an Al_2O_3 support has been investigated. It was established that:

- In NiMo citrate solutions, both in contact with the γ-Al_2O_3 support and without the support, the dominant phase is the heteropoly compound – ammonium 6-molybdonichelate $(NH_4)_4[NiMo_6O_{24}H_6]*nH_2O$.

- In CoMo citrate solutions that are not in contact with the γ-Al_2O_3 support sparingly soluble polymolybdate compounds are predominantly formed. Upon contact with γ-Al_2O_3 in CoMo systems, the formation of heteropoly compounds – ammonium 6-molybdocobaltite $(NH_4)_4[CoMo_6O_{24}H_6]*nH_2O$ and ammonium 6-molybdoaluminate $(NH_4)_3[AlMo_6O_{24}H_6]*nH_2O$ – is observed. Among these, the $(NH_4)_3[AlMo_6O_{24}H_6]*nH_2O$ phase predominates.

- Precipitate formation strongly depends on the concentration of the chelating agent (citric acid) in the impregnation solution. To ensure the stability of the impregnation solutions, the minimum required molar ratio of citric acid to promoter metal must be at least CA/Co ≥ 1.5 for CoMo citrate solutions and CA/Ni ≥ 1.8 for NiMo citrate solutions.

- The catalytic tests showed that the formation of HPCs precipitates does not reduce the HDS activity of the resulting catalysts. The higher activity observed is attributed to their higher actual loading of active metals, caused by the deposition of HPC particles on the alumina granules. Upon sulfidation, these species are converted into active sulfide particles and contribute to the overall catalytic activity. However, since the catalysts prepared with and without precipitate formation differ in their total metal content, the present data should not be interpreted as evidence for higher intrinsic activity of the precipitate-derived sulfide phase. The results demonstrate that precipitated HPCs can serve as an additional source of active metals, while their uncontrolled formation remains undesirable from the standpoint of reproducible industrial catalyst preparation.

Acknowledgements

The study was funded by the Russian Science Foundation according to the project No. 25-73-20153 (https://rscf.ru/en/project/25-73-20153/).

Supplementary data

- Supplementary data include SEM-EDX images, XRD, XPS, and Raman spectra; photos of catalysts and solutions in which heteropoly compounds have precipitated (DOCX);
- A video demonstrating the effect of citric acid concentration on the formation of heteropoly compounds in a Ni-Mo impregnation solutions (MOV).

Abbreviations

SRGO – straight-run gas oil

HDS – hydrodesulfurization

DMDS – dimethyl disulfide

EDTA – ethylenediaminetetraacetic acid

NTA – nitrilotriacetic acid

CA – citric acid

HPCs – heteropoly compounds

HMA – ammonium heptamolybdate

XRD – x-ray diffraction

SEM – scanning electron microscopy

References

[1] Shimizu T, Hiroshima K, Honma T, Mochizuki T, Yamada M. Highly active hydrotreatment catalysts prepared with chelating agents. Catal Today 1998;45:271–6. https://doi.org/10.1016/S0920-5861(98)00227-2.

[2] Li Y, Zhang T, Liu D, Liu B, Lu Y, Chai Y, et al. Study of the Promotion Effect of Citric Acid on the Active NiMoS Phase in NiMo/Al2O3 Catalysts. Ind Eng Chem Res 2019;58:17195–206. https://doi.org/10.1021/acs.iecr.9b02368.

[3] Nicosia D, Prins R. The effect of glycol on phosphate-doped CoMo/Al2O3 hydrotreating catalysts. J Catal 2005;229:424–38. https://doi.org/10.1016/J.JCAT.2004.11.014.

[4] Nicosia D, Prins R. The effect of phosphate and glycol on the sulfidation mechanism of CoMo/Al2O3 hydrotreating catalysts: an in situ QEXAFS study. J Catal 2005;231:259–68. https://doi.org/10.1016/J.JCAT.2005.01.018.

[5] Hensen EJM, de Beer VHJ, van Veen JAR, van Santen RA. A Refinement on the Notion of Type I and II (Co)MoS Phases in Hydrotreating Catalysts. Catal Letters 2002;84:59–67. https://doi.org/10.1023/A:1021024617582.

[6] Topsøe H. The role of Co–Mo–S type structures in hydrotreating catalysts. Appl Catal A Gen 2007;322:3–8. https://doi.org/10.1016/J.APCATA.2007.01.002.

[7] van Haandel L, Bremmer GM, Hensen EJM, Weber T. The effect of organic additives and phosphoric acid on sulfidation and activity of (Co)Mo/Al2O3 hydrodesulfurization catalysts. J Catal 2017;351:95–106. https://doi.org/10.1016/J.JCAT.2017.04.012.

[8] Simpson Howard D. Resid hydroprocessing catalyst and method of preparation. US-4886582-A, 1988.

[9] Majodina S, Walmsley R, Govender A, Hosten EC, Olivier J, Tshentu Z, et al. Influence of Ligands on the Surface Characteristics of CoMo/γ-Al2O3 and Hydrodesulfurization Catalytic Activity on Dibenzothiophene-Type Compounds. ChemistryOpen 2025;14:e202400123. https://doi.org/https://doi.org/10.1002/open.202400123.

[10] Chen J, Mi J, Li K, Wang X, Dominguez Garcia E, Cao Y, et al. Role of Citric Acid in Preparing Highly Active CoMo/Al2O3 Catalyst: From Aqueous Impregnation Solution to Active Site Formation. Ind Eng Chem Res 2017;56:14172–81. https://doi.org/10.1021/acs.iecr.7b02877.

[11] Klimov O V., Pashigreva A V., Bukhtiyarova GA, Budukva S V., Fedotov MA, Kochubey DI, et al. Bimetallic Co–Mo complexes: A starting material for high active hydrodesulfurization catalysts. Catal Today 2010;150:196–206. https://doi.org/10.1016/J.CATTOD.2009.07.095.

[12] Pashigreva A V., Bukhtiyarova GA, Klimov O V., Chesalov YA, Litvak GS, Noskov AS. Activity and sulfidation behavior of the CoMo/Al2O3 hydrotreating catalyst: The effect of drying conditions. Catal Today 2010;149:19–27. https://doi.org/10.1016/J.CATTOD.2009.07.096.

[13] Leonova KA, Klimov O V., Kochubey DI, Chesalov YA, Prosvirin IP, Larina T V., et al. Synthesis and characterisation of Co–Mo complexes containing the [Co(C2H8N2)3]2+ cation and [Mo2O7L]4− anion, where L is an oxalic, tartaric, citric or nitrilotriacetic acid residue. Polyhedron 2012;47:65–72. https://doi.org/10.1016/J.POLY.2012.08.025.

[14] Klimov OV, Koryakina GI, Budukva SV, Leonova KA, Pereyma VY, Dik PP, et al. Catalyst, method of producing support, method of producing catalyst and method of hydrofining hydrocarbon material. RU2472585C1, 2011.

[15] Klimov OV, Koryakina GI, Leonova KA, Budukva SV, Pereyma VY, Dik PP, et al. Method of preparing catalyst for hydropurification of hydrocarbon raw material. RU2534997C1, 2013.

[16] Bleta R, Schiavo B, Corsaro N, Costa P, Giaconia A, Interrante L, et al. Robust Mesoporous CoMo/γ-Al2O3 Catalysts from Cyclodextrin-Based Supramolecular Assemblies for Hydrothermal Processing of Microalgae: Effect of the Preparation Method. ACS Appl Mater Interfaces 2018;10:12562–79. https://doi.org/10.1021/acsami.7b16185.

[17] Lamonier C, Soogund D, Mazurelle J, Blanchard P, Guillaume D, Payen E. Origin of the dispersion limit in the preparation of Ni(Co)Mo/Al2O3 and Ni(Co)Mo/TiO2 HDS oxidic

precursors. Stud Surf Sci Catal 2006;162:713–20. https://doi.org/10.1016/S0167-2991(06)80972-9.

[18] van Veen JAR, de Wit H, Emeis CA, Hendriks PAJM. On the adsorption of heptamolybdate ions on γ-Al2O3 and TiO2. J Catal 1987;107:579–82. https://doi.org/10.1016/0021-9517(87)90323-X.

[19] Le Bihan L, Blanchard P, Fournier M, Grimblot J, Payen E. Raman spectroscopic evidence for the existence of 6-molybdoaluminate entities on an Mo/Al2O3 oxidic precursor. J Chem Soc{,} Faraday Trans 1998;94:937–40. https://doi.org/10.1039/A706359H.

[20] Bergwerff JA, Visser T, Leliveld G, Rossenaar BD, de Jong KP, Weckhuysen BM. Envisaging the Physicochemical Processes during the Preparation of Supported Catalysts: Raman Microscopy on the Impregnation of Mo onto Al2O3 Extrudates. J Am Chem Soc 2004;126:14548–56. https://doi.org/10.1021/ja040107c.

[21] Bergwerff J, Jansen M, Leliveld B, Visser T, Weckhuysen B. Influence of the preparation method on the hydrotreating activity of MoS_2/Al2O3 extrudates: A Raman micro spectroscopy study on the genesis of the active phase. J Catal 2006;243. https://doi.org/10.1016/j.jcat.2006.07.022.

[22] Humbert S, Devers E, Lesage C, Legens C, Lemaitre L, Sorbier L, et al. ASAXS study of the influence of sulfidation conditions and organic additives on sulfide slabs multiscale organization. J Catal 2021;395:412–24. https://doi.org/10.1016/J.JCAT.2021.01.033.

[23] Popovych OM, Budzulyak IM, Yukhymchuk VO, Budzulyak SI, Popovych DI. Raman spectroscopy of nickel molybdate and its modifications. Fullerenes, Nanotub Carbon Nanostructures 2021;29:1009–15. https://doi.org/10.1080/1536383X.2021.1925253.

[24] Muñoz M, Cabello CI, Botto IL, Minelli G, Capron M, Lamonier C, et al. Synthesis and spectroscopic 27Al NMR and Raman characterization of new materials based on the assembly of [AlO4Al12(OH)24(H2O)12]7+ isopolycation and Co–Cr and [AlMo6O24H6]3- Anderson heteropolyanions. J Mol Struct 2007;841:96–103.

https://doi.org/10.1016/J.MOLSTRUC.2006.11.067.

[25] Carrier X, Lambert JF, Che M. Ligand-Promoted Alumina Dissolution in the Preparation of MoOX/γ-Al2O3 Catalysts: Evidence for the Formation and Deposition of an Anderson-type Alumino Heteropolymolybdate. J Am Chem Soc 1997;119:10137–46. https://doi.org/10.1021/ja971981r.

[26] Botto IL, Garcia AC, Thomas HJ. Spectroscopical approach to some heteropolymolybdates with the anderson structure. J Phys Chem Solids 1992;53:1075–80. https://doi.org/10.1016/0022-3697(92)90081-N.

[27] Martin C, Lamonier C, Fournier M, Mentré O, Harlé V, Guillaume D, et al. Preparation and Characterization of 6-Molybdocobaltate and 6-Molybdoaluminate Cobalt Salts. Evidence of a New Heteropolymolybdate Structure. Inorg Chem 2004;43:4636–44. https://doi.org/10.1021/ic0354365.

[28] Himeno S, Niiya H, Ueda T. Raman Studies on the Identification of Isopolymolybdates in Aqueous Solution. Bull Chem Soc Jpn 1997;70:631–7. https://doi.org/10.1246/bcsj.70.631.

[29] Zhang S, Han M. Effect of synthesis pH on the structure and catalytic properties of FeMo catalysts. RSC Adv 2019;9:41720–8. https://doi.org/10.1039/C9RA07202K.

[30] Wang L, Hall WK. On the genesis of molybdena-alumina catalyst. J Catal 1980;66:251–5. https://doi.org/10.1016/0021-9517(80)90029-9.

[31] Benchrifa R, M. L, R. DE. Synthesis and crystal structure of two polymorphs of (NH4)2Mo4O13, orthorhombic (o) and triclinic (t). Eur J Solid State Inorg Chem 1989;26:593–601. https://doi.org/10.1002/chin.199029034.

[32] LI J, LUO Y, LI Z, ZHAO Z, LIU X, CHEN X, et al. Precise control and continuous production of β-ammonium tetramolybdate in concentric reactor. Trans Nonferrous Met Soc China 2024;34:309–21. https://doi.org/https://doi.org/10.1016/S1003-6326(23)66400-3.

[33] Böschen I, Buss B, Krebs B, Glemser O. Polymeric Octamolybdate Ions in the Crystal Structure of (NH4)6Mo8O27·4H2O. Angew Chemie Int Ed (in English) 1973;12:409.

https://doi.org/https://doi.org/10.1002/anie.197304091.

[34] Tytko K-H. Über den Mechanismus der Bildung von Polyanionen in wäßriger Lösung. Der Bildungsmechanismus des Polyoktamolybdations [Mo8O6-27]n / On the Mechanism for Polyanion Formation in Aqueous Solution. The Mechanism of Formation of the Polyoctamolybdate Ion [Mo8O 1973;28:272–5. https://doi.org/doi:10.1515/znb-1973-5-610.

[35] Klimov O V., Nadeina KA, Budukva S V., Avdeenko EA, Cherepanova S V., Chesalov YA, et al. Investigation of the regeneration of NiMoP/Al2O3 hydrotreating catalysts. Appl Catal A Gen 2022;630:118447. https://doi.org/10.1016/J.APCATA.2021.118447.

[36] Davydov AA, Goncharova OI. Use of IR spectroscopy in studies of catalysts based on molybdenum heteropoly compounds supported on oxides. Russ Chem Rev 1993;62:105. https://doi.org/10.1070/RC1993v062n02ABEH000008.

[37] Ayala-G M, Puello P E, Quintana P, González-García G, Diaz C. Comparison between alumina supported catalytic precursors and their application in thiophene hydrodesulfurization: $(NH_4)_4[NiMo_6O_{24}H_6]$·5H2O/γ-Al2O3 and NiMoOx/γ-Al2O3 conventional systems. RSC Adv 2015;5:102652–62. https://doi.org/10.1039/C5RA17695F.

[38] Courcot B, Bridgeman AJ. Structural and Vibrational Study of [Mo7O24]6− and $[W_7O_{24}]^{6-}$. J Phys Chem A 2009;113:10540–8. https://doi.org/10.1021/jp9063438.

[39] Davantès A, Lefèvre G. In situ characterization of (poly)molybdate and (poly)tungstate ions sorbed onto iron (hydr)oxides by ATR-FTIR spectroscopy. Eur Phys J Spec Top 2015;224:1977–83. https://doi.org/10.1140/epjst/e2015-02514-8.

[40] Lamonier C, Martin C, Mazurelle J, Harlé V, Guillaume D, Payen E. Molybdocobaltate cobalt salts: New starting materials for hydrotreating catalysts. Appl Catal B Environ 2007;70:548–56. https://doi.org/10.1016/J.APCATB.2005.12.027.

[41] Klimov O V., Pashigreva A V., Fedotov MA, Kochubey DI, Chesalov YA, Bukhtiyarova GA, et al. Co–Mo catalysts for ultra-deep HDS of diesel fuels prepared via synthesis of bimetallic surface compounds. J Mol Catal A Chem 2010;322:80–9.

https://doi.org/10.1016/J.MOLCATA.2010.02.020.

[42] Salomatina AA, Nadeina KA, Klimov O V, Danilova IG, Gerasimov EY, Prosvirin IP, et al. Influence of Ni/Mo Ratio on Structure Formation of Ni–Mo Complex Compounds in NiMo/Al2O3 Catalysts for Selective Diene Hydrogenation. Energy & Fuels 2022;36:15088–99. https://doi.org/10.1021/acs.energyfuels.2c02940.

[43] Murase K, Ando H, Matsubara E, Hirato T, Awakura Y. Determination of Mo(VI) Species and Composition in Ni-Mo Alloy Plating Baths by Raman Spectra Factor Analysis. J Electrochem Soc 2000;147:2210. https://doi.org/10.1149/1.1393509.

[44] Palcheva R, Kaluža L, Spojakina A, Jirátová K, Tyuliev G. NiMo/γ-Al2O3 Catalysts from Ni Heteropolyoxomolybdate and Effect of Alumina Modification by B, Co, or Ni. Chinese J Catal 2012;33:952–61. https://doi.org/10.1016/S1872-2067(11)60376-8.

[45] Lesage C, Devers E, Legens C, Roudenko O, Delpoux O, Beauvois A, et al. Speciation of the Oxide Phase of Molybdenum-Based HDS Catalysts Enhanced with Organic Additives Using an EXAFS/Raman Coupling Methodology. ChemCatChem 2025;17:e202401403. https://doi.org/https://doi.org/10.1002/cctc.202401403.

[46] Barata B, Legens C, Devers E, Delpoux O, Barthe L, Roudenko O, et al. Chemical Speciation by Quick-XAS and Raman Spectroscopy: Validation of Two Cells for in situ Time-Resolved Monitoring of the Impregnation and Drying of CoMoP/Al2O3 Catalysts. ChemCatChem 2023;15:e202201440. https://doi.org/https://doi.org/10.1002/cctc.202201440.

[47] Bremmer GM, van Haandel L, Hensen EJM, Frenken JWM, Kooyman PJ. The effect of oxidation and resulfidation on (Ni/Co)MoS2 hydrodesulfurisation catalysts. Appl Catal B Environ 2019;243:145–50. https://doi.org/10.1016/J.APCATB.2018.10.014.

[48] Vlasova EN, Bukhtiyarova GA, Deliy I V., Aleksandrov P V., Porsin AA, Panafidin MA, et al. The effect of rapeseed oil and carbon monoxide on SRGO hydrotreating over sulfide CoMo/Al2O3 and NiMo/Al2O3 catalysts. Catal Today 2020;357:526–33. https://doi.org/10.1016/J.CATTOD.2019.06.011.

[49] Yi X, Guo D, Li P, Lian X, Xu Y, Dong Y, et al. One pot synthesis of NiMo–Al2O3 catalysts by solvent-free solid-state method for hydrodesulfurization. RSC Adv 2017;7:54468–74. https://doi.org/10.1039/C7RA11892A.

[50] Scott CE, Perez-Zurita MJ, Carbognani LA, Molero H, Vitale G, Guzmán HJ, et al. Preparation of NiMoS nanoparticles for hydrotreating. Catal Today 2015;250:21–7. https://doi.org/10.1016/J.CATTOD.2014.07.033.

[51] Kaluža L, Palcheva R, Spojakina A, Jirátová K, Tyuliev G. Hydrodesulfurization NiMo catalysts supported on Co, Ni and B modified Al2O3 from Anderson heteropolymolybdates. Procedia Eng 2012;42:873–84. https://doi.org/10.1016/J.PROENG.2012.07.480.

[52] Nikulshin PA, Tomina NN, Pimerzin AA, Stakheev AY, Mashkovsky IS, Kogan VM. Effect of the second metal of Anderson type heteropolycompounds on hydrogenation and hydrodesulphurization properties of XMo6(S)/Al2O3 and Ni3-XMo6(S)/Al2O3 catalysts. Appl Catal A Gen 2011;393:146–52. https://doi.org/10.1016/J.APCATA.2010.11.033.

[53] Nikulshin PA, Mozhaev A V., Maslakov KI, Pimerzin AA, Kogan VM. Genesis of HDT catalysts prepared with the use of Co2Mo10HPA and cobalt citrate: Study of their gas and liquid phase sulfidation. Appl Catal B Environ 2014;158–159:161–74. https://doi.org/10.1016/J.APCATB.2014.04.013.

[54] Mozhaev A, Nikulshin P, Pimerzin A, Maslakov K, Pimerzin A. Investigation of co-promotion effect in NiCoMoS/Al2O3 catalysts based on Co2Mo10-heteropolyacid and nickel citrate. Catal Today 2016;271:80–90. https://doi.org/10.1016/j.cattod.2015.11.002.

[55] Blanchard P, Lamonier C, Griboval-Constant A, Payen E. New insight in the preparation of alumina supported hydrotreatment oxidic precursors: A molecular approach. Appl Catal A Gen 2007;322:33–45. https://doi.org/10.1016/j.apcata.2007.01.018.

The Figure Legend

Figure 1. XRD patterns of the precipitates: (a) CoMo-S1 and CoMo-S2; (b) NiMo-S1 and NiMo-S2.

Diffractograms of the precipitates obtained directly from the Co-Mo and Ni-Mo impregnation solutions, respectively (denoted CoMo-S1 and NiMo-S1), and after the impregnation solutions came into contact with the support (denoted CoMo-S2 and NiMo-S2)

Figure 2. Raman spectra of (a) CoMo-S1/S2 and (b) NiMo-S1/S2 samples

Raman spectra of the precipitates obtained directly from the Co-Mo and Ni-Mo impregnation solutions, respectively (denoted CoMo-S1 and NiMo-S1), and after the impregnation solutions came into contact with the support (denoted CoMo-S2 and NiMo-S2)

Figure 3. ATR-FTIR spectra of the CoMo-S1, CoMo-S2, NiMo-S1 and NiMo-S2

Figure 4. XRD patterns of the CoMo-1 and CoMo-2 catalysts

Diffractograms of Co-Mo catalysts obtained by impregnating the support with solutions having different CA/Co ratios. For the CoMo-1 catalyst, a solution with a CA/Co ratio of 1.2 was used, which resulted in the formation of a precipitate. For the CoMo-2 catalyst, a solution with a CA/Co ratio of 1.5 was used; no precipitate formed.

Figure 5. XRD patterns of the NiMo-1 and NiMo-2 catalysts

Diffractograms of Ni-Mo catalysts obtained by impregnating the support with solutions having different CA/Ni ratios. For the NiMo-1 catalyst, a solution with a CA/Ni ratio of 1.5 was used, which resulted in the formation of a precipitate. For the NiMo-2 catalyst, a solution with a CA/Ni ratio of 1.8 was used; no precipitate formed.

Figure 6. Raman microspectroscopy of CoMo-1. Image of an HPC crystal $(NH_4)_4[CoMo_6O_{24}H_6]$ and its Raman spectrum (top). Catalyst region free of $(NH_4)_4[CoMo_6O_{24}H_6]$ and its Raman spectrum (bottom).

Figure 7. Raman microspectroscopy of NiMo-1. Image of an HPC crystal of $(NH_4)_4[NiMo_6O_{24}H_6]$ and its Raman spectrum (top). Catalyst region free of HPCs $(NH_4)_4[NiMo_6O_{24}H_6]$ and its Raman spectrum (bottom).

Figure 8. SEM-EDX images of the surface of the CoMo-1 catalyst

Figure 9. SEM-EDX images of the surface of the CoMo-2 catalyst

Figure 10. SEM-EDX images of the surface of the NiMo-1 catalyst

Figure 11. Co2p (a) and Ni2p (b) spectra of the catalysts

Figure 12. SEM-EDX images of the surface of the sulfided NiMo-1 catalyst

Figure 13. Residual sulfur content (a) and HDS rate constant (b)

Supplementary Files

This is a list of supplementary files associated with this preprint. Click to download.

- SupportingInformation.docx
- Supportingvideo.mov